FKBP35 secures ribosome homeostasis in *Plasmodium falciparum*

Basil T. Thommen[1,2], Jerzy M. Dziekan[3], Fiona Achcar[4,5], Seth Tjia[3], Armin Passecker[1,2], Katarzyna Buczak[2], Christin Gumpp[1,2], Alexander Schmidt[2], Matthias Rottmann[1,2], Christof Grüring[1,2], Matthias Marti[4,5], Zbynek Bozdech[3], Nicolas M. B. Brancucci[1,2]

[1]Department of Medical Parasitology and Infection Biology, Swiss Tropical and Public Health Institute, 4123 Allschwil, Switzerland.

[2]University of Basel, 4001 Basel, Switzerland.

[3]School of Biological Sciences, Nanyang Technological University, Singapore.

[4]Wellcome Center for Integrative Parasitology, Institute of Infection, Immunity and Inflammation, University of Glasgow, Glasgow, UK.

[5]Institute for Parasitology, VetSuisse and Medical Faculty, University of Zurich, Zurich, Switzerland.

Correspondence:
Nicolas M. B. Brancucci, nicolas.brancucci@swisstph.ch

Keywords: malaria, *Plasmodium falciparum*, ribosome homeostasis, FKBP35, FK506, CETSA, antimalarial drugs

Abstract

Plasmodium falciparum is the most virulent malaria parasite and accounts for the majority of over 600'000 malaria-associated deaths annually. Parasites resistant to nearly all antimalarials have emerged, posing a serious threat to disease control efforts. The need for drugs with alternative modes of action is thus undoubted. The parasite's FKBP protein (*Pf*FKBP35) has gained attention as a promising drug target due to its high affinity to the macrolide compound FK506. Whilst there is considerable interest in targeting *Pf*FKBP35 with small molecules, a genetic validation of this factor as a drug target is missing. As a consequence, the function of *Pf*FKBP35 in live parasites remains elusive. Here, we report the generation of inducible knock-out, knock-down and over-expression cell lines and show that blood stage parasites require *Pf*FKBP35 for maintaining ribosome function. Limiting *Pf*FKBP35 levels are lethal to *P. falciparum* and result in a delayed-death phenotype that is characterized by defective ribosome homeostasis and protein translation. We furthermore show that, while FK506 is indeed binding to *Pf*FKBP35, the drug exerts it parasiticidal activity in a *Pf*FKBP35-independent manner and, using cellular thermal shift assays, we identify FK506-targets beyond *Pf*FKBP35. In addition to revealing first functional insights on the role of *Pf*FKBP35 in *P. falciparum* parasites, our

results show that current efforts to develop *Pf*FKBP35-targeting drugs need to be reconsidered urgently.

1 Introduction

Despite considerable progress in recent years, malaria remains one of the major global health threats (1). The apicomplexan parasite *Plasmodium falciparum* is responsible for the vast majority of the over 600'000 malaria deaths in 2020. Most of this burden is carried by infants and children under the age of five in sub-Saharan Africa. Malaria deaths increased by 12% compared to 2019, which can at least in part be explained by the COVID-19 related suspension of malaria control and treatment measures (1). In addition, the emergence of parasites resistant to most antimalarials, including artemisinin-based combination therapies, endangers current and future disease elimination efforts and underscores the need for developing drugs with alternative modes of action (2).

Symptomatic malaria is caused by the blood stage of infection. Here, parasites replicate asexually within host erythrocytes by multiple fission (schizogony). After completing schizogonic proliferation, infected red blood cells (RBCs) rupture and release daughter parasites ready to invade and replicate within new RBCs. Repeated intra-erythrocytic development cycles (IDC) allow parasites to rapidly expand in numbers and secure chronic infection. During each IDC, a small proportion of parasites commits to producing sexual stages, called gametocytes. These non-proliferative forms are required for transmission to the *Anopheles* insect vector and primary host of *P. falciparum*.

FK506 (tacrolimus), a well-characterized immunosuppressant, shows considerable activity against asexual blood stage parasites (3). *P. falciparum* encodes a single FK506-binding protein (FKBP) dubbed *Pf*FKBP35 (PF3D7_1247400), which is considered to be a promising drug target (4, 5). FKBPs belong to the immunophilin family and are conserved throughout the eukaryotic kingdom (6, 7). In contrast to the malaria parasite, most other eukaryotes encode several FKBPs that, besides showing high affinity for the FK506 drug, exert peptidyl-prolyl isomerase (PPIase) activity. The PPIase moiety catalyzes cis-trans isomerization of proline residues – an event thought to be rate-limiting for the folding of many proteins (8). Independent of their PPIase activity, FKBPs act as chaperones to prevent protein aggregation under stress conditions (9, 10). Furthermore, some FKBP variants play a role in cellular signaling through regulatory interactions with receptors, including the ryanodine receptor, the inositol

69 triphosphate receptor as well as receptors of the TGF beta type I family (11-13), or by
70 controlling the trafficking of the GTPase H-Ras between the plasma membrane and the Golgi
71 apparatus (14). Besides signaling, certain FKBPs exert gene regulatory functions by interacting
72 with histone deacetylases or by serving as transcription factors of genes encoding ribosomal
73 proteins (15, 16). While the four FKBPs in yeast show high functional redundancy (17), the 18
74 human isoforms are involved in diverse cellular processes. *Hs*FKBP12 for instance is best-
75 known for its ability to form a complex with the immunosuppressant drugs FK506 and
76 rapamycin. These complexes inhibit the phosphatase activity of calcineurin and the kinase
77 activity of mTOR (mechanistic target of rapamycin), respectively (18). Amongst many other
78 effects, this inhibition results in decreased T-cell activation. Of note, the regulatory role of
79 *Hs*FKBP12 depends on the presence of rapamycin or FK506. In absence of drugs, this
80 immunophilin neither interacts with mTOR nor with calcineurin and does hence not affect
81 activity of these key components of eukaryotic cells. Due to the conserved nature of FKBPs,
82 rapamycin and FK506 have also gained attention as potential antimicrobial drugs (3, 7).

83 Similar to its homologs in model organisms, *Pf*FKBP35 harbors PPIase and chaperoning
84 activity *in vitro* (5). Despite sharing key features with FKBPs of other eukaryotes, its role in *P.*
85 *falciparum* remains elusive. *Pf*FKBP35 is believed to interact with heat shock proteins (HSPs)
86 and co-immunoprecipitates with cytoskeletal factors of *P. falciparum* (19). While *Pf*FKBP35
87 is inhibiting the phosphatase activity of recombinant calcineurin in a FK506-independent
88 manner (20-22), it does not co-localize with calcineurin *in vivo* (21). The protein is expressed
89 throughout the 48-hour intra-erythrocytic development of *P. falciparum* and is found within the
90 cytosol of ring stage parasites. In the older trophozoite and the replicating schizont stages, the
91 protein was reported to also localize to the nucleus (21). While a transposon-based mutagenesis
92 screen suggests that *Pf*FKBP35 is essential for intra-erythrocytic replication (23), neither its
93 cellular function nor its essentiality was confirmed experimentally in live parasites. The
94 unknown role in parasite biology notwithstanding, *Pf*FKBP35 is considered to be a viable drug
95 target and, given the fact that *P. vivax* and *P. knowlesi* encode FKBP homologs that exhibit
96 comparable PPIase activities (24, 25), future FKBP-targeted therapies may be effective across
97 different *Plasmodium* species.

98 Crystal structures of *Pf*FKBP35 in complex with FK506 and rapamycin revealed high affinity
99 interactions with the FK506-binding domain of the protein (20, 26, 27). Consistent with these
100 observations, *in vitro* enzyme activity assays showed that FK506 inhibits the PPIase activity of
101 recombinant *Pf*FKBP35 in a dose-dependent manner (5). Previous research aimed at exploiting

102 structural differences between human and parasite-encoded FKBPs to circumvent the
103 immunosuppressive activity of drug-bound *Hs*FKBP12 (28-31). These efforts include
104 investigation of non-covalent FKBP inhibitors such as adamantyl derivatives, macrocycles, the
105 small molecule D44 (28-30, 32, 33) and the synthetic ligand for FKBP (SLF) as well as
106 derivatives thereof designed to covalently bind *Pf*FKBP35 (34). While D44 shows promising
107 antimalarial activity, it fails to alter thermostability of the FK506-binding domains of
108 *Pf*FKBP35 and *Hs*FKBP12 *in vitro* (34), suggesting that this compound does not directly
109 interact with *Pf*FKBP35.

110 Up until now, *Pf*FKBP35 has not been validated as a drug target using reverse genetics, and the
111 link between *Pf*FKBP35-interacting drugs and their antimalarial activity remains elusive (3).
112 Interestingly, treatment with FK506 causes a transcriptional response in *P. falciparum* similar
113 to that of the calcineurin inhibitor cyclosporin A, suggesting that the antimalarial activity of
114 FK506 is ultimately explained by calcineurin de-regulation (27). By contrast, the work of
115 Monaghan and colleagues indicated that the effects of FK506 are caused by the direct inhibition
116 of *Pf*FKBP35, rather than through recruiting drug-*Pf*FKBP35 complexes to other cellular
117 targets (35). Clearly, reverse genetics efforts are needed, not only to inform current and future
118 drug development approaches, but also to clarify the function of *Pf*FKBP35 in *P. falciparum*.

119 Here, we generated inducible *Pf*FKBP35 knock-out, knock-down as well as over-expression
120 cell lines and show that *Pf*FKBP35 is essential for asexual replication of blood forms. We
121 demonstrate that *Pf*FKBP35 is vital for ribosome homeostasis on the post-transcriptional level
122 and likely acts as a chaperone during the biogenesis of ribosomes in the nucleus. As a result,
123 *Pf*FKBP35 knock-out parasites stall protein translation prior to dying at the early schizont stage,
124 which underpins the potential of *Pf*FKBP35 as a drug target. Using cellular thermal shift assays
125 (CETSA), we corroborate the high affinity binding of FK506 to *Pf*FKBP35 and reveal
126 interactions of the *Pf*FKBP35/FK506 pair with ribosome-associated proteins. Importantly,
127 however, our data demonstrate that FK506 fails at inhibiting the essential function of
128 *Pf*FKBP35 and exerts its antimalarial activity in a *Pf*FKBP35-independent manner. While this
129 has major implications for the development of future FK506-based antimalarials and/or
130 *Pf*FKBP35-inhibiting drugs, we identify putative targets of FK506 beyond *Pf*FKBP35 in *P.*
131 *falciparum*.

132

133

134 # 2 Results

135 ## 2.1 *Pf*FKBP35 is essential for asexual replication

136 In a first step, using CRISPR/Cas9-mediated gene editing, we engineered a *P. falciparum* cell
137 line allowing for a conditional knock-down of *Pf*FKBP35 using the DD/Shield system (36, 37)
138 (Figs. 1A and S1A-B). Despite the efficient depletion of *Pf*FKBP35 under knock-down
139 conditions, parasites did not show apparent growth defects (Figs. S1C-D). Immunofluorescence
140 assays (IFA) showed that *Pf*FKBP35 localizes to distinct foci within the parasite nucleus (Fig.
141 1B).

142 Next, we generated a cell line allowing for the conditional knock-out of the endogenous coding
143 sequence using a dimerizable Cre recombinase (DiCre)-based system (38). Specifically, we
144 introduced two *loxP* sites – one within a synthetic intron (39) downstream of the start codon
145 and one after the stop codon of the *fkbp35* coding region – and added a *green fluorescent protein*
146 (*gfp*) sequence downstream of this expression cassette (Figs. 2A, S2A). As a result, these
147 NF54/iKO-FKBP35 parasites express tag-free, wild-type (WT) *Pf*FKBP35 protein under
148 control conditions (FKBP35^{WT}). Upon DiCre activation, the *loxP* sites are recombined and the
149 *fkbp35* locus is excised from the parasite genome (Figs. 2A, S2B). Under these knock-out
150 conditions (FKBP35^{KO}), parasites express cytosolic GFP under control of the endogenous
151 *fkbp35* promoter. This setup allows monitoring knock-out efficiency at the single cell level and
152 revealed that DiCre successfully deleted *fkbp35* in the vast majority of parasites (Fig. 2B).

153 In a first attempt, we induced the *fkbp35* knock-out in synchronous ring stage NF54/iKO-
154 FKBP35 parasites at 0-6 hours post erythrocyte invasion (hpi), i.e. prior to the expected peak
155 transcription of *fkbp35* (40). These FKBP35^{KO} parasites showed a delayed death phenotype:
156 parasites completed intra-erythrocytic development in the first generation (G1) without
157 noticeable effects (Fig. 2C) and entered the next generation (G2) with a multiplication rate
158 similar to that of the FKBP35^{WT} control population (Fig. 2D). In G2, however, FKBP35^{KO}
159 parasites arrested at the late trophozoite/early schizont stage (approximately 30-36 hpi) with
160 many cells failing to enter DNA replication in the S-phase (Fig. 2C). To investigate this
161 phenomenon in more detail, we induced the *fkbp35* knock-out at three different time points
162 during the IDC. Similar to DiCre activation at 0-6 hpi, knocking out *fkbp35* at 12-18 hpi resulted
163 in parasite death at the trophozoite/schizont stage of the subsequent generation. However, when
164 induced at 24-30 hpi or 34-40 hpi in G1, parasites did not only complete the current IDC but
165 also successfully passed through G2 before they eventually arrested in G3 (Fig. 2E).
166 Considering that low *Pf*FKBP35 levels are sufficient to maintain the essential function of the

167 protein, as observed with the NF54/iKD-FKBP35 parasites (see Fig. S1C, D), it is conceivable
168 that proteins expressed between 0 and 24hpi, i.e. prior to deleting *fkbp35* from the genome,
169 allow parasites to enter G3.

170 The delayed death of FKBP35^{KO} is reminiscent of a phenotype observed in apicoplast-deficient
171 parasites (41, 42). We therefore tested if *Pf*FKBP35 is involved in apicoplast biology, but did
172 not find evidence for an association with this organelle (Fig. S2C). Furthermore, given the
173 reported interaction of *Pf*FKBP35 with heat shock proteins (19, 21), we also tested the parasite`s
174 response to heat stress, but could not detect altered heat-susceptibility between FKBP35^{KO} and
175 FKBP35^{WT} cells (Fig. S2D).

176

177 **2.2 *Pf*FKBP35 is crucial for ribosome homeostasis and protein translation**

178 To further elucidate the function of *Pf*FKBP35, we induced the *fkbp35* knock-out in early ring
179 stages (0-6 hpi) and compared the proteomes of FKBP35^{KO} and FKBP35^{WT} parasites at the
180 schizont stage of G1 (36-42 hpi) and at the trophozoite stage of the following generation (G2,
181 24-30 hpi) using a quantitative proteomics approach.

182 *The knock-out of PfFKBP35 causes accumulation of pre-ribosome components in G1*

183 Consistent with the efficient deletion of *fkbp35* on the genomic level, FKBP35^{KO} schizonts of
184 G1 showed a 19-fold (18.9 +/-5.7 s.d.) reduction of FKBP35 and GFP levels were increased by
185 84-fold (83.7 +/-38.5 s.d.) when compared to the control population (Fig. 3A, Table S1).
186 Besides *Pf*FKBP35 and GFP, 50 parasite proteins were significantly deregulated in FKBP35^{KO}
187 schizonts and 34 of them found at elevated levels compared to the FKBP35^{WT} control
188 conditions. A gene ontology analysis using PANTHER (43) indicated enrichment of the "*pre-*
189 *ribosome*" (fold enrichment = 30.4, p-value = 1.46E-5, 4/34 proteins) and "*nucleolus*" (fold
190 enrichment = 6.77, p-value = 8.85E-4, 5/34 proteins) terms among these factors. While the pre-
191 ribosome is a large subunit precursor of mature ribosomes, the nucleolus represents the primary
192 site for the biogenesis of ribosomal subunits (44). In contrast to factors being more abundant in
193 knock-out parasites, none of the 16 factors with lower abundance in FKBP35^{KO} cells were
194 associated with ribosome-related processes (Table S1). Despite being phenotypically silent in
195 G1, the accumulation of pre-ribosome and nucleolar components hints at perturbed ribosome
196 maturation in these cells. Specifically, it is conceivable that the observed buildup of ribosome
197 intermediates results from reduced anabolic activity, i.e. the stalling of nucleolar pre-ribosome
198 assembly.

199 Notwithstanding these effects, FKBP35^{KO} cells were equally sensitive to the translation
200 inhibitor cycloheximide compared to their FKBP35^{WT} counterparts (Fig. 3B), indicating that
201 ribosome function is not compromised at this point in time (45). This is consistent with normal
202 cell cycle progression in G1 and unaltered multiplication rates of FKBP35^{KO} parasites, as
203 described above (see Figs. 2C-D), and shows that the prominent depletion of *Pf*FKBP35 does
204 not have a major impact on parasite viability in G1.

205

206 *PfFKBP35 is essential for maintaining normal levels of functional ribosomes in G2*

207 In the following generation (G2, 24-30 hpi), the proteome of FKBP35^{KO} trophozoites showed
208 substantial differences. Despite the absence of morphological changes at this point in time, 216
209 proteins were significantly deregulated (Fig. 3C). Among these, 50 proteins were found at
210 higher abundance compared to FKBP35^{WT} and their gene ontology terms point towards an
211 effect on processes involved in energy metabolism (Fig. 3D).

212 The majority of deregulated factors (166 of 216) in G2, however, were less abundant in
213 FKBP35^{KO} compared to the FKBP35^{WT} control cells. Very prominently, 20 of the top 50 hit
214 molecules are ribosomal proteins that, on average, show a two-fold reduction (2.0 +/- 0.4 s.d.)
215 in FKBP35^{KO} parasites (Table S1). It is therefore not surprising that PANTHER identified the
216 knock-out of *Pf*FKBP35 to mainly affect ribosome-related processes, such as "*cytoplasmic*
217 *translation*", "*ribosome assembly*", and "*ribosomal large subunit biogenesis*" (Fig. 3D) (43).

218 To assess if the reduced levels of ribosomal proteins result in lower protein translation rates,
219 we employed the "surface sensing of translation" (SUnSET) technique. SUnSET is based on
220 incorporation of the tyrosyl-tRNA analogue puromycin into nascent peptide chains and thereby
221 allows monitoring newly synthesized proteins (46). As expected, we found that FKBP35^{KO}
222 trophozoites in G2 (24-30 hpi) showed reduced translation rates compared to the FKBP35^{WT}
223 control population (Fig. 3E). Further, protein synthesis was not affected in parasites of the
224 parental line NF54/DiCre following DiCre activation using rapamycin (S2E), demonstrating
225 that translation is impaired in response to knocking out *Pf*FKBP35.

226 Taken together, these results indicate that, under knock-out conditions, *Pf*FKBP35 levels
227 become limiting for ribosome maturation late during schizogony of G1, without having
228 immediate effects on the steady-state levels of mature ribosomes. The knock-out of *Pf*FKBP35
229 is thus phenotypically silent in G1. In absence of a continuous supply of mature ribosomes

230 under FKBP35^{KO} conditions, however, FKBP35^{KO} parasites fail at synthesizing protein at
231 levels that would support normal parasite development in the next generation (G2).

232

233 **2.3 The knock-out of *Pf*FKBP35 is transcriptionally silent**

234 In model organisms, FKBPs are involved in diverse cellular processes. Besides prominent
235 activities in protein folding, trafficking and receptor signaling, FKBPs can also affect
236 transcriptional regulation, for instance by controlling translocation of transcription factors into
237 the nucleus as well as by direct binding to DNA and transcriptional regulators, such as histone
238 modifying enzymes (15, 16, 47).

239 We thus reasoned that the altered proteome FKBP35^{KO} parasites may be the result of
240 *Pf*FKBP35-controlled transcription. To examine whether *Pf*FKBP35 is involved in *P.*
241 *falciparum* gene regulation, we compared the transcriptional profiles of FKBP35^{WT} and
242 FKBP35^{KO} in a time course RNA-Sequencing (RNA-Seq) experiment spanning two IDCs.
243 Specifically, we induced the knock-out of FKBP35 in synchronous parasites at 0-6 hpi and
244 collected RNA from parasite populations at three and four subsequent time points (TPs) in G1
245 and G2, respectively (Figs. 4A, S3A). With the exception of TP7, these time points cover a time
246 frame during which FKBP35^{KO} cells cannot be distinguished from their FKBP35-expressing
247 counterparts on a morphological level (compare Fig. 2).

248 As expected, the transcriptome of FKBP35^{KO} showed a prominent reduction of steady-state
249 *fkbp35* transcripts already in TP1 (11.3-fold +/-2.0 s.d.) compared to the FKBP35^{WT} control
250 population (Fig. S3B, Table S2). During peak transcription at 30-36 hpi (TP2), this difference
251 increased to 240-fold (238.4 +/-20.0 s.d.) and, consistent with the efficient recombination at the
252 *fkbp35* locus, these cells started transcribing *gfp*. Notwithstanding the prominent depletion of
253 *fkbp35* transcripts, the transcriptome of FKBP35^{KO} is only marginally affected up to and
254 including 24-30 hpi in G2 (TP6). By contrast, at 30-36 hpi (TP7) the transcription of knock-out
255 parasites shows major changes (Fig. 4B). Considering the appearance of morphological changes
256 in FKBP35^{KO} at this time point, effects on the transcriptome are unlikely to represent specific
257 activities of *Pf*FKBP35 in gene regulation. Indeed, mapping the transcriptome of individual
258 time points to a high resolution reference (48), revealed a significant slow-down of FKBP35^{KO}
259 compared to FKBP35^{WT} parasites at TP7 (Figs. 4C, S3C). This indicates aborted cell cycle
260 progression in FKBP35^{KO} parasites during a phase that is characterized by a rapid increase in
261 biomass – possibly due to a translation and/or size-dependent cell cycle checkpoint (49). At

262 earlier time points (TP1-TP6), the transcriptomes of FKBP35^{KO} and FKBP35^{WT} are
263 comparable and the differences observed on the level of individual genes clearly fail at
264 explaining the proteomic changes observed in FKBP35^{KO} parasites at 24-30 hpi in G2 (TP6),
265 reiterating that the essential activity of *Pf*FKBP35 is linked to post-transcriptional processes.

266

267 **2.4 FKBP-targeting drugs fail at inhibiting the essential function of *Pf*FKBP35**

268 *Pf*FKBP35 emerged as a promising antimalarial drug target (4) and considerable efforts were
269 made to define interactions of this immunophilin with small molecules in the last decade (29-
270 31, 35). Several studies conclusively demonstrated that FK506 – the most well-known ligand
271 of mammalian FKBPs (50) – binds to *Pf*FKBP35 (20, 26, 27) and kills asexual blood stage
272 parasites with a half-maximal inhibitory concentration (IC50) in the low micromolar range at
273 1.9 µM (3).

274 Considering the proposed direct interaction between FK506 and FKBP35 in *P. falciparum*, we
275 expected that FKBP35^{KO} parasites show altered sensitivity to the drug. Consistent with
276 published data, FK506 killed FKBP35^{WT} cells with an IC50 of 1942 nM (+/-193 nM s.d.) when
277 administered at 0-6 hpi (Fig. 5A). Surprisingly however, and despite the prominent depletion
278 of the protein under knock-out conditions, FKBP35^{KO} and FKBP35^{WT} parasites were equally
279 sensitive to FK506 (IC50 = 1741 +/- 187) (Fig. 5A). Similarly, neither the efficient knock-down
280 of *Pf*FKBP35 in NF54/iKD-FKBP35 parasites (compare Fig. S1C), nor its over-expression
281 (OE) in NF54/iOE-FKBP35 cells (Fig. S4A-C), resulted in the expected sensitivity change to
282 FK506 treatment (Fig. 5B). In addition to this apparent independence of the drug to varying
283 *Pf*FKBP35 levels, and in agreement with earlier studies (3, 29, 51), FK506 unfolds its
284 antimalarial activity fairly quickly, i.e. within the same cycle after treatment. Standing in stark
285 contrast to the delayed death phenotype of FKBP35^{KO} parasites (compare Fig. 2), this
286 immediate activity on parasite survival substantiates the notion that FK506 must target essential
287 parasite factors other than *Pf*FKBP35.

288 To rule out that the timing of drug exposure is masking expected links between FK506 and
289 *Pf*FKBP35, we tested whether administering FK506 at 30-36 hpi (instead of 0-6 hpi) affects
290 parasite survival in a *Pf*FKBP35-dependent manner. However, we did not observe a change
291 compared to FKBP35^{WT} parasites (Fig. S5A), ruling out the possibility that FKBP35^{KO}
292 parasites were killed by FK506 before *Pf*FKBP35 levels were different in the two populations.
293 Further, to account for a scenario in which the activity of FK506 on *Pf*FKBP35 is masked by a

294 temporal delay between drug exposure and parasite killing, we induced the knock-out of
295 *Pf*FKBP35 at 34-40 hpi (instead of 0-6 hpi) and allowed FKBP35^{KO} parasites to proceed to G2,
296 before exposing them to different FK506 concentrations. Despite these efforts, FKBP35^{WT} and
297 FKBP35^{KO} parasites were equally sensitive to FK506 (Fig. S5B, S5C).

298 In model eukaryotes, FK506 binds FKBP and the thereby formed complex inhibits calcineurin
299 – a phosphatase involved in controlling cellular immune responses (52). To clarify if FK506
300 treatment is ultimately targeting the *P. falciparum* homolog of calcineurin as proposed (27), we
301 performed dose-response experiments with the calcineurin-specific inhibitor cyclosporin A. No
302 difference in cyclosporin A sensitivity could be observed between FKBP35^{KO} and FKBP35^{WT},
303 indicating that this drug inhibits parasite growth independent of *Pf*FKBP35, which is in line
304 with previous reports (21, 35) (Fig. S5D). Drug interaction experiments further revealed the
305 absence of additive effects between cyclosporin A and 1.5 µM FK506 (0.75 x IC50),
306 irrespective of whether FKBP35^{KO} or FKBP35^{WT} parasites were exposed to the drugs,
307 demonstrating that the *Pf*FKBP35/FK506 pair does not inhibit calcineurin activity (Fig. S5E).
308 However, similar to FK506, cyclosporin A is only active in the micromolar range and may
309 therefore not be suitable for the evaluation of specific enzyme inhibition in *P. falciparum.*

310 In addition to FK506, we evaluated the *Pf*FKBP35-specific inhibitor D44 (N-(2-Ethylphenyl)-
311 2-(3h-Imidazo[4,5-B]pyridin-2-Ylsulfanyl)acetamide) but, surprisingly, we failed to reproduce
312 the previously reported dose-response effect (29). We tested D44 from two suppliers using
313 NF54/iKO-FKBP35, NF54 wild type and K1 parasite strains using different assay setups,
314 including the gold standard method that is based on the incorporation of tritium labeled
315 hypoxanthine into DNA of replicating cells (53). Still, we could not detect any activity of D44
316 on asexual replication of blood stage parasites (Figs. S5F-G).

317 Taken together, these results are in clear conflict with the perception that FK506 and D44 target
318 the essential activity of *Pf*FKBP35.

319

320 **2.5 Probing FK506 interactions in Cellular Thermal Shift Assays (CETSA)**

321 Considering the unaltered activity of FK506 in FKBP35^{KO} compared to FKBP35^{WT} parasites,
322 we reasoned that FK506 must target proteins other than *Pf*FKBP35. To identify potential targets
323 of the drug in *P. falciparum*, we used the *cellular thermal shift assay followed by mass*
324 *spectrometry* (MS-CETSA). This approach exploits the fact that, once drug-protein complexes

325 are formed, thermostability of the target protein is altered (54). We applied the so-called
326 *isothermal dose-response* variant of CETSA using FK506 (55). Here, target proteins are
327 identified based on their dose-dependent stabilization by drugs under thermal challenge
328 (different temperatures) when compared to a non-denaturing condition (37 °C), using the
329 change in the area under the curve (ΔAUC) and the dose-response curve goodness of fit (R^2) as
330 metrics (Fig. 5C) (55).

331 *CETSA identifies putative targets of FK506*

332 In a first step, we performed CETSA in combination with drug-exposed protein extracts. Since
333 proteins lose their physiological context during the process of protein extraction, this variant of
334 the CETSA approach is designed to identify direct protein-drug interactions (54, 55). Not
335 surprisingly, we found *Pf*FKBP35 to be stabilized by FK506 in a dose-dependent manner when
336 challenged at 60 °C with an EC50 of 152.0 nM (Fig. 5D). The fact that FK506 exhibits its
337 stabilizing activity already in the low nanomolar concentration range indicates high affinity
338 interactions between the protein-drug pair. This FK506-mediated stabilization of *Pf*FKBP35 is
339 thus achieved at drug concentrations that are magnitudes below the IC50 of FK506 in parasite
340 survival assays (1942 nM +/-193 nM s.d.) (compare Fig. 5A). In line with several previous
341 reports on the *Pf*FKBP35/FK506 pair *in vitro*, our results show that, indeed, FK506 is binding
342 to *Pf*FKBP35, but in contrast to previous assumptions this interaction fails at explaining the
343 antimalarial activity of FK506.

344 Besides *Pf*FKBP35, FK506 stabilizes a number of other proteins in a dose-dependent manner
345 (Figs. 5E and S6). A few of these factors show pronounced sigmoidal stabilization profiles and
346 are predicted to be essential (Fig. 5E) (23). Amongst others, N6-methyl transferase MT-A70
347 (PF3D7_0729500), histone deacetylase HDA2 (PF3D7_1008000), pre-mRNA-splicing factor
348 CEF1 (PF3D7_1033600), FeS cluster assembly protein SufD (PF3D7_1103400) and the
349 H/ACA ribonucleoprotein complex subunit 1 (PF3D7_1309500) showed most pronounced
350 stabilization profiles (Fig. S6 and Table S3). In contrast to *Pf*FKBP35, most of these likely
351 essential candidates are stabilized at FK506 concentrations close to the drug`s IC50 (compare
352 Fig. 5A). It is therefore tempting to speculate that the binding of FK506 to at least one of these
353 factors is responsible for the antimalarial activity of the drug.

354 *Live cell CETSA reveals proteins interacting with the PfFKBP35/FK506 pair*

355 Given the high-affinity interaction of *Pf*FKBP35 with FK506 and its association with ribosomal
356 proteins, we set out to describe the native context of *Pf*FKBP35 using the live cell variant of

357 CETSA. In contrast to focusing exclusively on direct protein-drug interactions, live cell CETSA
358 allows capturing drug-induced shifts in protein stability beyond those of direct binding partners
359 (55) and amongst others allows identifying factors present in the same protein complex as the
360 target protein. To do so, CETSA takes advantage of the fact that factors within complexes have
361 similar denaturation temperatures due to their co-aggregation upon heat-induced denaturation
362 (56). As a consequence, this CETSA variant generally identifies more factors compared to the
363 protein extract-based CETSA approach (Fig. 5C).

364 As expected, and confirming the results above, live cell CETSA shows that FK506 alters the
365 thermal stability of *Pf*FKBP35 already at very low drug concentrations when challenged at 60
366 °C with an EC50 of 286.7 nM (Fig. 5D). Interestingly, and in contrast to the protein lysate-
367 based approach, live cell CETSA revealed that more than 50 ribosomal proteins are stabilized
368 in presence of FK506 when challenged at 55°C, with a median EC50 of 45.9 nM (25th percentile
369 = 34.2, 75th percentile = 58.9). Of note, these ribosomal proteins were stabilized at virtually
370 identical FK506 concentrations (Figs. 5F, and S7), indicating that the drug – directly or
371 indirectly – interacts with ribosomal complexes. This is in further agreement with the fact that
372 these ribosomal factors were not identified by protein lysate-based CETSA (compare Figs. 5C,
373 S6).

374 Worth mentioning, we observed a drug dose-dependent increase in soluble protein abundance
375 of ribosomal factors also under non-denaturing conditions, i.e. at 37 °C, with a median EC50
376 of 1.94 µM (25th percentile = 1.85, 75th percentile = 2.1) (Figs. 5F, S7). Generally, due to the
377 absence of a denaturing heat challenge, such a drug-dependent enrichment in soluble protein
378 levels does not indicate binding-induced thermal stabilization of proteins (55). Instead, this can
379 be the result of increased protein synthesis, altered protein conformation or, alternatively, occur
380 in response to factors disengaging from larger protein complexes. The fact that FK506
381 solubilizes a high number of ribosomal proteins within a very narrow concentration window
382 also at 37 °C, further substantiates the notion that these individual factors are liberated from the
383 same ribosomal complex or from complexes that interact with each other and shows that FK506
384 negatively affects stability of ribosomal structures in live cells. However, these effects are
385 limited to high, presumably saturating FK506 concentrations, likely explaining why the drug
386 fails at killing parasites in a *Pf*FKBP35-dependent manner. Importantly, the vast majority of
387 ribosomal proteins identified in live cell CETSA are shared with those de-regulated in
388 *Pf*FKBP35 knock out cells (Fig. 5G), providing conclusive evidence for a shared localization
389 of FK506 and its *Pf*FKBP35 target in live parasites.

390 Together with the above-described importance of *Pf*FKBP35 in ribosome homeostasis, these
391 results strongly suggest that FK506 is recruited to the activity site of *Pf*FKBP35 – most
392 probably the nucleolar maturation sites of ribosomes – where it leads to a destabilization of
393 ribosomal complexes.

394

395 # 3 Discussion

396 Members of the FKBP family are involved in regulating diverse cellular processes in eukaryotic
397 as well as in prokaryotic cells (8, 57). FKBPs are characterized by the presence of at least one
398 FK506-binding domain that serves as the binding site for proline and proline-analogs, including
399 FK506 and rapamycin, and as the active site for catalyzing prolyl peptide bond isomerization.
400 In contrast to most other eukaryotes, the human malaria parasite *P. falciparum* encodes a single
401 FKBP only (21). The enzymatic activity of *Pf*FKBP35, as well as the interactions of the protein
402 with FKBP-targeting drugs, was subject to considerable drug-focused research *in vitro*. Besides
403 demonstrating the drug`s affinity to *Pf*FKBP35 by co-crystallization, these efforts uncovered
404 that FK506 inhibits enzymatic activity of the protein`s PPIase domain (5). Together with the
405 anti-malarial activity of FK506, these data offered compelling evidence for an essential but yet
406 uncharacterized role of *Pf*FKBP35 during blood stage development of *P. falciparum*.

407 Here, we set out to investigate the role of *Pf*FKBP35 in parasite biology. Using an inducible
408 knock-out approach, we show that *Pf*FKBP35 is indeed essential for intra-erythrocytic
409 development of asexually replicating *P. falciparum* parasites and FKBP35^{KO} cells die during
410 the late trophozoite/early schizont stage. Surprisingly, these parasites display a delayed-death
411 phenotype that is independent of apicoplast function and only manifests in the cycle following
412 knock-out induction without affecting cell cycle progression in the first generation (G1) or
413 multiplication rates from G1 to G2. This contradicts the known effects of FK506 and other
414 *Pf*FKBP35-targeting drugs for two main reasons. First, these drugs exert their parasiticidal
415 activity within the same IDC (29). Second, neither the conditional knock-out, knock-down nor
416 the overexpression of *Pf*FKBP35 altered the parasite's sensitivity to FK506, even though levels
417 of the *Pf*FKBP35 target are profoundly deregulated in the respective mutant lines. Together,
418 these data show that the parasite-killing activity of FK506 is independent of the essential
419 function of *Pf*FKBP35. We hence aimed at the identification of other FK506 targets using
420 CETSA, as discussed further down.

421 Knocking out *Pf*FKBP35 early during intra-erythrocytic development has no effect on parasite
422 morphology in G1 and provokes only moderate changes on the protein level compared to
423 FKBP35^{WT} parasites. While the effects in G1 are relatively subtle, it is noticeable that
424 nucleolus-associated factors are found at higher abundance in knock-out cells. In the next cycle,
425 FKBP35^{KO} parasites show a dramatic decrease of factors associated with ribosome- and
426 translation-related processes during trophozoite development (G2, 24-30 hpi). Consistently,
427 protein translation in FKBP35^{KO} parasites is reduced considerably. Importantly, at this point in
428 time, FKBP35^{KO} cells still show ordinary morphology and their transcriptional activity remains
429 largely unaffected. The observed changes in the abundance of ribosomal factors must therefore
430 result from post-transcriptional activity of *Pf*FKBP35. While ribosomal components are present
431 at higher levels in G1, they are drastically reduced in FKBP35^{KO} cells in G2. These opposing
432 effects are peculiar, but likely result from *Pf*FKBP35 activity in a shared cellular process.
433 Specifically, it is conceivable that low *Pf*FKBP35 levels inhibit ribosome maturation in G1,
434 explaining the accumulation of (pre-) ribosomal factors. While the levels of functional
435 ribosomes are sufficient to support continued translation in G1, ribosomes likely become
436 limiting in the next generation (G2), which eventually results in stalled translation activity and
437 concomitant parasite death at the onset of schizogony; i.e. at a time when protein synthesis is
438 required for facilitating the steep increase in biomass.

439 In contrast to the significant effects on the protein level, the transcription of FKBP35^{KO} remains
440 largely unaffected by the loss of *Pf*FKBP35 and becomes apparent only during late
441 trophozoite/early schizont development in G2 (30-36 hpi); i.e. at a time during which cell cycle
442 progression is slowed down in FKBP35^{KO} parasites. In fact, at this stage the transcriptional
443 signature of FKBP35^{KO} parasites is dominated by the slowed progression through intra-
444 erythrocytic development, rather than resulting from specific gene regulatory events. While this
445 stalling is consistent with the observed effects on ribosome homeostasis and protein translation,
446 it demonstrates that, in contrast to certain FKBP family members in other organisms,
447 *Pf*FKBP35 does not have apparent roles in transcriptional control.

448 As discussed above, binding of FK506 to *Pf*FKBP35 cannot explain the drug's antimalarial
449 activity and our attempts to identify targets of FK506 using resistance selection failed. This
450 indicates that parasites do not readily acquire resistance mutations, possibly due to drug action
451 on multiple targets (58). We hence aimed at identifying other FK506 targets using CETSA. In
452 line with previous work on the drug *in vitro*, CETSA on *P. falciparum* protein extracts
453 confirmed that FK506 is targeting *Pf*FKBP35 with exceptionally high affinity in the low

454 nanomolar range. Considering this well-characterized FK506-*Pf*FKBP35 interaction (27) and
455 the resulting inhibition of its PPIase activity (5), unaltered drug sensitivity of *Pf*FKBP35
456 mutants indicates that PPIase activity is dispensable for blood stage parasites. Noteworthy,
457 PPIase-independent functions of FKBPs have been described in other systems. For instance,
458 PPIase activity of the *Escherichia coli* trigger factor (TF), a ribosome-associated FKBP, is not
459 required for protein folding (59). Similarly, human FKBP52 maintains its function as a
460 chaperone under PPIase-inhibiting conditions (9). While it is conceivable that PPIase activity
461 is dispensable for intra-erythrocytic development of *P. falciparum*, the enzymatic activity of
462 *Pf*FKBP35 may be compensated by other factors, e.g. by PPIase domain-harboring members
463 of the cyclophilin family (60).

464 CETSA performed on protein lysates identified a number of parasite factors binding to FK506.
465 Compared to the *Pf*FKBP35/FK506 pair, however, these interactions are of considerably lower
466 affinity. The adenosine-methyltransferase MT-A70 (PF3D7_0729500) and the pre-mRNA-
467 splicing factor CEF1 (PF3D7_1033600), for instance, were stabilized by FK506 with EC50
468 concentrations of 2.0 and 3.1 µM, respectively. While this affinity is relatively poor compared
469 to the strong interaction formed between *Pf*FKBP35 and FK506, one should be cautious
470 designating the binding of FK506 to these proteins as irrelevant "*off target*" effects. In fact,
471 their inhibition may well be masked by high-affinity binding of FK506 to *Pf*FKBP35 – a
472 possibility that shall briefly be discussed in the following section.

473 Assuming that FK506 is inhibiting the essential function of *Pf*FKBP35, one would expect
474 parasites to show a delayed-death phenotype similar to that observed in FKBP35$^{\mathbf{KO}}$ parasites.
475 In contrast to this delayed killing, the effect of FK506 on other essential targets likely manifests
476 in the same cycle and would hence mask the effect of *Pf*FKBP35-inhibition. Consistent with
477 this possibility, FK506 kills *P. falciparum* parasites at 1.9 µM (+/-0.2 µM s.d.), i.e. at
478 concentrations similar to those required for stabilizing MT-A70 and CEF1 under thermal
479 challenge in CETSA. Our attempts to prove that FK506 indeed inhibits essential functions of
480 *Pf*FKBP35 failed: Neither knocking out *Pf*FKBP35 at different time points nor adding FK506
481 to different stages of FKBP35$^{\mathbf{KO}}$ parasites could provide evidence for a scenario in which
482 *Pf*FKBP35-dependent effects are simply masked by "*off target*" effects (compare Fig. S5). This
483 indicates that either the binding of FK506 does not interfere with the essential role of
484 *Pf*FKBP35, or that *Pf*FKBP35 is inhibited only at high FK506 concentrations that also inhibit
485 other essential factors. In this context it is worth mentioning that parasites remain unaffected
486 by a highly efficient knock-down of endogenous *Pf*FKBP35 (observed with NF54/iKD-

487 FKBP35; compare Figs. S1C-D), which demonstrates that very low protein levels are sufficient
488 to maintain the essential function of *Pf*FKBP35. It is thus conceivable that high FK506
489 concentrations are required to fully inhibit *Pf*FKBP35 – a view that is further supported by data
490 obtained with the live cell CETSA approach.

491 Besides identifying direct binding of drugs to their target, live cell CETSA allows capturing
492 indirect effects on factors that act in the same pathway or in the same protein complex as the
493 drug-bound target (55). While this approach confirmed the high affinity binding of FK506 to
494 *Pf*FKBP35, it also revealed that more than 50 ribosomal proteins share a very prominent
495 CETSA signature: First, they are thermally stabilized by FK506 within a narrow concentration
496 window of the drug. Second, higher levels of FK506 increase the solubility of these ribosomal
497 components also at 37 °C. These results indicate that the FK506/*Pf*FKBP35 pair interacts with
498 ribosomal complexes and that FK506 is able to induce the dissociation of these ribosomal
499 structures under physiological conditions. Importantly, and in contrast to the binding of FK506
500 to *Pf*FKBP35, this effect on ribosomes is only observed at high concentrations of the drug.
501 Together, these data likely explain the discrepancy observed between the high binding affinity
502 of FK506 for *Pf*FKBP35 and the low or even absent effect of the drug on *Pf*FKBP35 function
503 in blood stage parasites.

504 Furthermore, neither live cell CETSA (Fig. S5H) nor drug interaction experiments using FK506
505 and the calcineurin inhibitor cyclosporin A provided evidence for interactions between
506 *Pf*FKBP35 and the phosphatase calcineurin. Given that calcineurin is essential for RBC
507 invasion (51) and is inhibited by recombinant *Pf*FKBP35 in an FK506-independent manner
508 (21), *Pf*FKBP35 depletion should alleviate the effect of cyclosporin A on parasite invasion.
509 However, no *Pf*FKBP35-dependent effect could be observed, questioning whether *Pf*FKBP35
510 indeed controls calcineurin activity *in vivo*.

511 In line with our data, previous biochemical approaches revealed potential links between
512 *Pf*FKBP35 and ribosomes. Using co-immunoprecipitation, Leneghan and colleagues revealed
513 that *Pf*FKBP35 is interacting with 480 proteins, of which 31 are ribosomal factors (19). Indeed,
514 FKBP family members are essentially involved in controlling ribosomes in other systems. The
515 human FKBP variant *Hs*FKBP25, for instance, is recruited to the pre-ribosome where its
516 chaperone activity appears to be required for the assembly of the ribosomal large subunit (61).
517 While the FKBP variant of yeast, Fpr4, interacts with the ribosome biogenesis factor Nop53
518 (62), the *Escherichia coli* trigger factor (TF) is part of the ribosomal complex and crucial for
519 the folding of nascent proteins (63, 64). Intriguingly, a delayed death phenotype very similar to

520 that of FKBP35^{KO}, has been described following exposure of *P. falciparum* parasites to the
521 antibiotic tunicamycin: Whereas treatment of ring stage parasites neither affected parasite
522 development in the first generation nor invasion of daughter cells into new RBCs, parasites died
523 at approximately 30 hpi in the next cycle (65, 66). Tunicamycin is known to interfere with the
524 processing of the 7S rRNA of the 40S subunit in yeast and hence blocks ribosome maturation
525 (67). Considering the marked reduction of ribosomal factors in FKBP35^{KO} parasites, it is
526 tempting to speculate that *Pf*FKBP35 is chaperoning ribosome biogenesis similar to Fpr4 and
527 FKBP25 in *Saccharomyces cerevisiae* and *humans*, respectively.

528 The fact that *Pf*FKBP35 localizes to distinct nuclear foci and its depletion causes dysregulation
529 of ribosomes points towards a role within the nucleolus – the nuclear compartment driving
530 ribosome biogenesis (44). Using IFAs, we found that *Pf*FKBP35 does not co-localize with the
531 nucleolar marker fibrillarin (68) (Fig. S8). However, its localization appears to be intertwined
532 with that of this rRNA methyltransferase. Specifically, *Pf*FKBP35 is mostly found in close
533 vicinity to fibrillarin-rich regions. Nucleoli in eukaryotic cells generally consist of two or, in
534 higher eukaryotes, three sub-compartments. Of those, the granular component (GC) represents
535 the site of pre-ribosome assembly and encompasses fibrillarin-enriched central regions of
536 nucleoli (69). The spatial correlation observed between *Pf*FKBP35 and fibrillarin may thus
537 indicate localization to different sub-nucleolar compartments, with *Pf*FKBP35 occupying the
538 GC area of the nucleolus.

539

540 In summary, we demonstrate that limiting *Pf*FKBP35 levels are lethal to *P. falciparum* and
541 result in a delayed-death phenotype that is characterized by perturbed ribosome homeostasis
542 and defective protein translation, which is likely linked to the reduced biogenesis of functional
543 ribosomes in the nucleolus. We further show that FKBP-binding drugs, including FK506, exert
544 their parasiticidal activity in a *Pf*FKBP35-independent manner, urging strong caution for the
545 future development of FKBP-targeting antimalarials, especially when based on FK506 and
546 structural derivatives thereof. In addition to revealing first insights into the essential function
547 of *Pf*FKBP35 in ribosome homeostasis of *P. falciparum*, we are convinced that the presented
548 data offer valuable information for target-based efforts in malaria drug discovery.

549

550 # 4 Methods

551 ## 4.1 Parasite culture

552 *P. falciparum* culture and synchronization was performed as described (70, 71). Parasites were
553 cultured in AB+ or B+ human red blood cells (Blood Donation Center, Zürich, Switzerland) at
554 a hematocrit of 5% in culture medium containing 10.44 g/L RPMI-1640, 25 mM HEPES, 100
555 µM hypoxanthine, 24 mM sodium bicarbonate, 0.5% AlbuMAX II (Gibco #11021-037), 0.1
556 g/L neomycin, and 2 mM choline chloride (Sigma #C7527). To achieve stabilization of DD-
557 tagged proteins in the cell lines NF54/iKD-FKBP35 and NF54/iOE-FKBP35, parasites were
558 cultured in presence of 625 nM Shield-1 (36, 37). To induce the DiCre-mediated recombination
559 of *loxP* sites in NF54/iKO-FKBP35 parasites, cultures were split and treated for 4 h with 100
560 nM rapamycin or the corresponding volume DMSO, which served as vehicle control, giving
561 rise to $FKBP35^{KO}$ and $FKBP35^{WT}$ populations, respectively (38). Cultures were gassed with
562 3% O_2, 4% CO_2 and 93% N_2 and incubated in an airtight incubation chamber at 37°C.

563

564 ## 4.2 Cloning of transfection constructs

565 CRISPR/Cas9-based gene editing of the NF54 parasites was performed using a two-plasmid
566 approach as previously described (72, 73). This system is based on co-transfection of a plasmid
567 that contains the expression cassettes for the Cas9 enzyme, the single guide RNA (sgRNA) and
568 the blasticidin deaminase (BSD) resistance marker (pBF-gC), and a pD-derived donor plasmid
569 that contains the template for the homology-directed repair of the Cas9-induced DNA double
570 strand break (Fig. S2A) (73).

571 The plasmids pBF-gC_FKBP-3', pBF-gC_FKBP-5' and pBF-gC_P230p targeting the 3' or 5'
572 end of *fkbp35* (PF3D7_1247400) or the *p230p* (PF3D7_0208900) locus (74), respectively, were
573 generated by ligation of two annealed oligonucleotides (gRNA_top and gRNA_bottom) into
574 the BsaI-digested pBF-gC backbone (73) using T4 DNA ligase (New England Biolabs).

575 The donor plasmid pD_FKBP35-iKO was generated by assembling six DNA fragments in a
576 Gibson reaction (75) using (i) the plasmid backbone amplified by polymerase chain reaction
577 (PCR) from pUC19 (primers PCRa_F/PCRa_R) (73), (ii/iii) the 5' and 3' homology regions
578 amplified from genomic DNA (primers PCRb_F/PCRb_R and PCRc_F/PCRc_R,
579 respectively), (iv) the *green fluorescent protein* (*gfp*) sequence amplified from pHcamGDV1-
580 GFP-DD (primers PCRd_F/PCRd_R) (73), (v) the HRPII terminator amplified from genomic
581 DNA (primers PCRe_F/PCRe_R), and (vi) the *fkbp35* sequence containing an artificial *loxPint*

582 (39) amplified from a *P. falciparum* codon-optimized synthetic sequence (primers
583 PCRf_F/PCRf_R) ordered from Genscript.

584 The donor plasmid pD_FKBP35-iKD was generated by assembling five DNA fragments in a
585 Gibson reaction (75) using (i) the plasmid backbone amplified from pUC19 (primers
586 PCRa_F/PCRa_R) (73), (ii/iii) the 5' and 3' homology regions amplified from genomic DNA
587 (primers PCRg_F/PCRg_R and PCRh_F/PCRh_R, respectively), (iv) the *gfp* sequence
588 amplified from pHcamGDV1-GFP-DD (primers PCRi_F/PCRi_R) (73), and (v) the
589 destabilization domain (*dd*) sequence amplified from pHcamGDV1-GFP-DD (primers
590 PCRj_F/PCRj_R) (73).

591 The donor plasmid pD_FKBP35-iOE was generated by assembling three DNA fragments in a
592 Gibson reaction (75) using (i) the NheI/PstI-digested plasmid pkiwi003 (76), (ii) the *fkbp35*
593 coding sequence amplified from genomic DNA (primers PCRk_F/PCRk_R), and (iii) the *gfp-*
594 *dd* sequence amplified from pHcamGDV1-GFP-DD (primers PCRl_F/PCRl_R) (73).

595 Oligonucleotides are listed in Table S4.

596

597 **4.3 Transfection and selection of gene-edited parasites**

598 *P. falciparum* transfection using the CRISPR/Cas9 two-plasmid approach was performed as
599 described previously (73). Briefly, 50 µg of each plasmid (pBF-gC_FKBP-3' and pD_FKBP35-
600 iKO, pBF-gC_FKBP-5' and pD_FKBP35-iKD, pBF-gC_P230p and pD_FKBP35-iOE) were
601 co-transfected into an NF54::DiCre line (77), in which *ap2-g* was tagged with the fluorophore
602 mScarlet as described previously (78). Transgenic parasites were selected with 2.5 µg/mL
603 blasticidin-S-hydrochloride, which was added 24 h after transfection for 10 days. Transgenic
604 populations were usually obtained 2-3 weeks after transfection and correct editing of the
605 modified loci was confirmed by PCR on gDNA (Figs. S1B, S2B and S4B). Primer sequences
606 used for these PCRs are listed in Table S4. Clonal parasite lines were obtained by limiting
607 dilution cloning (79).

608

609 **4.4 DNA content analysis**

610 NF54/iKO-FKBP35 parasites were fixed in 4% formaldehyde/0.0075% glutaraldehyde for 30
611 min at room temperature and washed 3 times in PBS and stored at 4°C. Samples were collected

612 from three independent biological replicates. RNA was digested by incubation with 0.1 mg/mL
613 RNAse A in PBS containing 0.1% Triton-X100 for 15 min at room temperature. Nuclei were
614 stained using 1X SYBR Green 1 DNA stain (Invitrogen S7563) for 20 min and washed three
615 times in PBS. The fixation step quenched the GFP signal detected by the flow cytometer (Fig.
616 S9). SYBR Green intensity was measured using a MACS Quant Analyzer 10 and analyzed
617 using the FlowJo_v10.6.1 software.

618

619 **4.5 Western blotting**

620 Saponin lysis of 500 µL infected red blood cells at 3-5% parasitaemia was performed by
621 incubation for 10 min on ice in 3 mL ice-cold 0.15% saponin in PBS. The parasite pellets were
622 washed two times in ice-cold PBS and resuspended in Laemmli buffer (62.5 mM Tris base, 2%
623 SDS, 10% glycerol and 5% 2-mercaptoethanol). Proteins were separated on 4-12% Bis-Tris
624 gels (Novex, Qiagen) using MOPS running buffer (Novex, Qiagen). Then proteins were
625 transferred to a nitrocellulose membrane (GE healthcare #106000169), which was blocked with
626 5% milk powder in PBS/0.1% Tween (PBS-T) for 1 h. The membrane was probed using the
627 primary antibodies mAb mouse α-GFP (1:1'000, Roche Diagnostics #11814460001), mAb
628 mouse α-*Pf*GAPDH (1:20'000) (80), or mAb mouse α-puromycin (1:5'000, Sigma MABE343)
629 diluted in blocking solution. After 2 h incubation, the membrane was washed 5 times in PBS-
630 T before it was incubated with the secondary antibody goat α-mouse IgG (H&L)-HRP
631 (1:10'000, GE healthcare #NXA931). After 1 h incubation, the membrane was washed 5 times
632 and the signal was detected using the chemiluminescent substrate SuperSignal West Pico Plus
633 (Thermo Scientific, REF 34580) and the imaging system Vilber Fusion FX7 Edge 17.10 SN.
634 Nitrocellulose membranes were stripped by incubating for 10 min in a stripping buffer (1 g/L
635 SDS, 15 g/L glycine, 1% Tween-20, pH 2.2) and washed three times in PBS-T before blocking
636 and re-probing.

637

638 **4.6 Drug dose-response experiments**

639 Dose-response relationships were assessed by exposing synchronous ring stage parasites at
640 0.5% parasitaemia and 1.25% hematocrit to 12 drug concentrations using a two-step serial
641 dilution in 96-well plates (Corning Incorporated, 96-well cell culture plate, flat bottom, REF
642 3596) in three independent biological replicates. The plates were gassed and incubated for 48
643 h at 37 °C. FK506 (MedChemExpress HY-13756), D44 (ChemBridge 7934155 and ChemDiv

644 7286-2836) and cyclosporin A (Sigma 30024) stocks of 10 mM were prepared in DMSO and
645 working solutions were prepared immediately before the experiment. To measure parasite
646 survival using flow cytometry, cultures were stained in 1X SYBR Green 1 DNA stain
647 (Invitrogen S7563) in a new 96-well plate (Corning Incorporated, 96-well cell culture plate,
648 round bottom, REF 3788) and incubated in the dark for 20 min. The samples were washed once
649 in PBS. Using a MACS Quant Analyzer 10, 50'000 events per condition were measured and
650 analyzed using the FlowJo_v10.6.1 software. Infected RBCs were identified based on SYBR
651 Green 1 DNA stain intensity. The gating strategy is shown in Fig. S9. To quantify parasite
652 survival based on hypoxanthine incorporation into DNA, compounds were dissolved in DMSO (10
653 mM), diluted in hypoxanthine-free culture medium and titrated in duplicates over a 64-fold range (6 step
654 twofold dilutions) in 96 well plates. 100 µl asexual parasite culture (prepared in hypoxanthine-free
655 medium) were added to each well and mixed with the compound to obtain a final haematocrit of 1.25%
656 and a final parasitemia of 0.3%. After incubation for 48 hrs, 0.25 µCi of [3H]-hypoxanthine was added
657 per well and plates were incubated for an additional 24 hrs. Parasites were then harvested onto glass-
658 fiber filters using a Microbeta FilterMate cell harvester (Perkin Elmer, Waltham, US) and radioactivity
659 was counted using a MicroBeta2 liquid scintillation counter (Perkin Elmer, Waltham, US). The results
660 were recorded and expressed as a percentage of the untreated controls. Curve fitting and IC50
661 calculations were performed using a non-linear, four-parameter regression model with variable
662 slope (Graph Pad Prism, version 8.2.1).

663

664 **4.7 Fluorescence microscopy**

665 To localize *Pf*FKBP35, NF54/iKD-FKBP35 parasites were fixed in 4% formaldehyde/0.0075%
666 glutaraldehyde for 30 min at room temperature and washed three times in PBS. The fixed cells
667 were permeabilized by incubation with 0.1% Triton-X100-containing PBS for 15 min. After
668 two washing steps in PBS, the cells were incubated in a blocking/aldehyde quenching solution
669 (3% BSA in PBS complemented with 50 mM ammonium chloride). The samples were
670 incubated with the primary antibodies rabbit α-GFP (1:400, Abcam ab6556) and mAb mouse
671 α-fibrillarin (1:100, Santa Cruz Biotechnology sc-166021) for 1 h in 3% BSA in PBS and
672 washed 3 times in PBS. Subsequently, the samples were incubated with the secondary
673 antibodies goat α-rabbit IgG (H&L) Alexa Fluor 488 (1:250, Invitrogen A11008) and goat a-
674 mouse IgG (H&L) Alexa Fluor 594 (1:250, Invitrogen A11032), for 1 h and washed 3 times,
675 before they were mixed with Vectashield containing DAPI (Vector laboratories, H-1200), and

676 mounted on a microscopy slide. Slides were imaged using a Leica THUNDER 3D Assay
677 imaging system.

678

679 **4.8 Proteomics**

680 Parasite cultures were split at 0-6 hpi in G1 and treated for 4 h with 100 nM rapamycin. Saponin
681 lysis of paired FKBP35^{WT} and FKBP35^{KO} populations at 36-42 hpi in G1 and 24-30 hpi in G2
682 was performed as described above. Samples were collected in three independent biological
683 replicates. The washed parasite pellet was snap frozen in liquid nitrogen. After thawing,
684 parasites were resuspended in 25 µL of lysis buffer (5% SDS, 100 mM tetraethylammonium
685 bromide (TEAB), 10 mM tris(2-carboxyethyl)phosphin (TCEP), pH 8.5) and sonicated (10
686 cycles, 30 sec on/off at 4 °C, Bioruptor, Diagnode). Lysates were subsequently reduced for 10
687 minutes at 95 °C. Samples were then cooled down to RT and 0.5 µL of 1M iodoacetamide was
688 added to the samples. Cysteine residues were alkylated for 30 min at 25 °C in the dark.
689 Digestion and peptide purification was performed using S-trap technology (Protifi) according
690 to the manufacturer's instructions. In brief, samples were acidified by addition of 2.5 µL of
691 12% phosphoric acid (1:10) and then 165 µL of S-trap buffer (90% methanol, 100 mM TEAB
692 pH 7.1) was added to the samples (6:1). Samples were briefly vortexed and loaded onto S-trap
693 micro spin-columns (Protifi) and centrifuged for 1 min at 4000 g. Flow-through was discarded
694 and spin-columns were then washed 3 times with 150 µL of S-trap buffer (each time samples
695 were centrifuged for 1 min at 4000 g and flow-through was removed). S-trap columns were
696 then moved to the clean tubes and 20 µL of digestion buffer (50 mM TEAB pH 8.0) and trypsin
697 (at 1:25 enzyme to protein ratio) were added to the samples. Digestion was allowed to proceed
698 for 1h at 47 °C. Then, 40 µL of digestion buffer were added to the samples and the peptides
699 were collected by centrifugation at 4000 g for 1 minute. To increase the recovery, S-trap
700 columns were washed with 40 µL of 0.2% formic acid in water (400g, 1 min) and 35 µL of
701 0.2% formic acid in 50% acetonitrile. Eluted peptides were dried under vacuum and stored at -
702 20 °C until further analysis.

703 Peptides were resuspended in 0.1% aqueous formic acid and peptide concentration was adjusted
704 to 0.25 µg/µL. 1 µL of each sample was subjected to LC-MS/MS analysis using an Orbitrap
705 Elicpse Tribrid Mass Spectrometer fitted with an Ultimate 3000 nano system (both from
706 Thermo Fisher Scientific) and a custom-made column heater set to 60 °C. Peptides were
707 resolved using a RP-HPLC column (75 µm × 30 cm) packed in-house with C18 resin (ReproSil-

708 Pur C18–AQ, 1.9 µm resin; Dr. Maisch GmbH) at a flow rate of 0.3 µL/min. The following
709 gradient was used for peptide separation: from 2% buffer B to 12% B over 5 min, to 30% B
710 over 40 min, to 50% B over 15 min, to 95% B over 2 min followed by 11 min at 95% B then
711 back to 2% B. Buffer A was 0.1% formic acid in water and buffer B was 80% acetonitrile, 0.1%
712 formic acid in water.

713 The mass spectrometer was operated in DDA mode with a cycle time of 3 seconds between
714 master scans. Each master scan was acquired in the Orbitrap at a resolution of 240,000 FWHM
715 (at 200 m/z) and a scan range from 375 to 1600 m/z followed by MS2 scans of the most intense
716 precursors in the linear ion trap at "Rapid" scan rate with isolation width of the quadrupole set
717 to 1.4 m/z. Maximum ion injection time was set to 50 ms (MS1) and 35 ms (MS2) with an AGC
718 target set to 1e6 and 1e4, respectively. Only peptides with charge state 2-5 were included in the
719 analysis. Monoisotopic precursor selection (MIPS) was set to Peptide, and the Intensity
720 Threshold was set to 5e3. Peptides were fragmented by HCD (Higher-energy collisional
721 dissociation) with collision energy set to 35%, and one microscan was acquired for each
722 spectrum. The dynamic exclusion duration was set to 30 seconds.

723 The acquired raw-files were imported into the Progenesis QI software (v2.0, Nonlinear
724 Dynamics Limited), which was used to extract peptide precursor ion intensities across all
725 samples applying the default parameters. The generated mgf-file was searched using MASCOT
726 against a *Plasmodium falciparum* (isolate 3D7) database (Uniprot, 11.2019) and 392 commonly
727 observed contaminants using the following search criteria: full tryptic specificity was required
728 (cleavage after lysine or arginine residues, unless followed by proline); 3 missed cleavages were
729 allowed; carbamidomethylation (C) was set as fixed modification; oxidation (M) and acetyl
730 (Protein N-term) were applied as variable modifications; mass tolerance of 10 ppm (precursor)
731 and 0.6 Da (fragments). The database search results were filtered using the ion score to set the
732 false discovery rate (FDR) to 1% on the peptide and protein level, respectively, based on the
733 number of reverse protein sequence hits in the dataset. Quantitative analysis results from label-
734 free quantification were processed using the SafeQuant R package v.2.3.2 (81) to obtain peptide
735 relative abundances. This analysis included global data normalization by equalizing the total
736 peak/reporter areas across all LC-MS runs, data imputation using the knn algorithm, summation
737 of peak areas per protein and LC-MS/MS run, followed by calculation of peptide abundance
738 ratios. Only isoform specific peptide ion signals were considered for quantification. To meet
739 additional assumptions (normality and homoscedasticity) underlying the use of linear
740 regression models and t-Tests, MS-intensity signals a were transformed from the linear to the

741 log-scale. The summarized peptide expression values were used for statistical testing of
742 between condition differentially abundant peptides. Here, empirical Bayes moderated t-Tests
743 were applied, as implemented in the R/Bioconductor limma package (82). The resulting per
744 protein and condition comparison *p*-values were adjusted for multiple testing using the
745 Benjamini-Hochberg method.

746 Gene ontology enrichment analysis was performed using the PANTHER Overrepresentation
747 Test with the correction method "False Discovery Rate", the test type "Fisher's Exact", and the
748 annotation data set "PANTHER GO-Slim" (43).

749

750 **4.9 IPP complementation**

751 Parasite cultures were split at 0-6 hpi in G1 and treated for 4 h with 100 nM rapamycin.
752 FKBP35^{KO} and FKBP35^{WT} populations were split again and supplemented either with 200 µM
753 isopentenyl pyrophosphate (IPP) (Sigma I0503) or the corresponding volume H_2O. The
754 respective culture medium was replaced daily. Parasites treated with 156 ng/mL doxycycline
755 (Sigma D9891) were used to confirm that IPP complementation is able to rescue apicoplast-
756 deficient parasites. DNA content analysis was performed as described above.

757

758 **4.10 Heat shock susceptibility testing**

759 Parasites cultures were split at 0-6 hpi in G1 and treated for 4 h with 100 nM rapamycin. While
760 control populations were always incubated at 37 °C, test populations were incubated at 40 °C
761 for 6 h starting at 24-30 hpi. Parasitaemia was measured in G2 using flow cytometry as
762 described above.

763

764 **4.11 Surface sensing of translation (SUnSET)**

765 Parasite cultures were split at 0-6 hpi in G1 and treated for 4 h with 100 nM rapamycin. At 24-
766 30 hpi in G2, the cultures were incubated with 1 µg/mL puromycin (Sigma P8833) for 1 h at
767 37 °C (46, 83). Saponin lysis and Western blotting were performed as described above.

768

769 ### 4.12 Cellular thermal shift assay (CETSA)

770 The mass spectrometry-based isothermal dose-response cellular thermal shift assay (ITDR-MS-
771 CETSA) was performed according to the protocol developed by Dziekan and colleagues (55).
772 Briefly, live parasites (10^7 MACS-purified trophozoites per condition) were exposed to a
773 FK506 (MedChemExpress HY-13756) concentration gradient (100 µM to 1.5 nM) and a
774 DMSO control for 1 h. Subsequently, the parasites were washed in PBS and exposed to the
775 denaturing temperatures 50 °C, 55 °C and 60 °C as well as to a non-denaturing temperature 37
776 °C for 3 min, before they were cooled down to 4 °C for 3 min. Afterwards, the cells were lysed
777 by resuspending in a lysis buffer (50 mM HEPES pH 7.5, 5 mM β-glycerophosphate, 0.1 mM
778 Na_3VO_4, 10 mM $MgCl_2$, 2 mM TCEP, and EDTA-free protease inhibitor cocktail (Sigma)),
779 three freeze/thaw cycles, and mechanical shearing using a syringe with a 31-gauge needle.
780 Subsequently, insoluble proteins were pelleted by centrifugation (20 min at 4 °C and 20'000 g)
781 and the soluble fraction was collected and subjected to protein digestion, reduction, alkylation,
782 and TMT10 labelling followed by LC/MS analysis as described (55).

783 To prepare the protein lysate, saponin-lysed parasites were lysed in the afore-mentioned buffer
784 by three freeze/thaw cycles and mechanical shearing. After centrifugation, soluble proteins
785 were exposed to a FK506 concentration gradient (200 µM to 3 nM) and a DMSO control for 1
786 min before the thermal challenge was performed as described above. Afterwards, the soluble
787 protein fraction was isolated and prepared for by LC/MS analysis as described (55).

788 Data analysis was performed using the Proteome Discoverer 2.1 software (Thermo Fisher
789 Scientific) and the R package "mineCETSA" (v 1.1.1). Only proteins identified by at least three
790 peptide spectrum matches (PSMs) were included in the analysis (55).

791

792 ### 4.13 Transcriptomics

793 #### 4.13.1 Sample preparation

794 The RNA of 500 µL iRBCs at 3-5% parasitaemia was isolated using 3 mL TRIzol reagent
795 (Invitrogen) followed by purification using the Direct-zol RNA MiniPrep kit (Zymo). Samples
796 were collected from three biological replicates. Stranded RNA sequencing libraries were
797 prepared using the Illumina TruSeq stranded mRNA library preparation kit (REF 20020594)
798 according to the manufacturer's protocol. The library was sequenced in 100 bp paired-end reads

799 on an Illumina NextSeq 2000 sequencer using the Illumina NextSeq 2000 P3 reagents (REF
800 20040560), resulting in 5 million reads on average per sample.

801 **4.13.2 RNA-Seq data analysis**

802 Fastqc was run on all raw fastq files. Then, each file was aligned with hisat2 (version 2.0.5)
803 (84) against the 3D7 reference genome (PlasmoDB v58) (85) in which the GFP and the recoded
804 FBPK35 sequences were added at the end of chromosome 12. Read counts for each gene and
805 for each sample were then counted using featureCount (gff file from PlasmoDB v58 modified
806 to include the added GFP and FBPK35). TPM (Transcripts Per Kilobase Million) were then
807 calculated from the raw count matrix.

808 Principal component analysis (PCA) was performed using the R (version 4.2.1) function
809 prcomp using log transformed TPMs. PCA revealed that the rapamycin-treated replicate B of
810 TP 3 ("3B.R") was a clear outlier and is different from any other replicate at any time point
811 (Fig. S3D). For this reason, it was excluded from further analysis. The PCA was done again
812 without it and the other samples show the same pattern as the initial PCA (Fig. S3E).

813 DESeq2 (version 1.36) (86) was used for normalization and differential expression analysis.
814 Paired differential expression tests where done for each time point using DESeq2 LRT
815 (likelihood ratio test) using the full model ~ Treatment + Replicate (Treatment is DMSO or
816 Rapamycin and Replicate is the clone, added as the data is paired) and the reduced model ~
817 Replicate. From this paired test and the average log fold-change calculated from the TPMs,
818 normalized volcano plots were made using the R package EnhancedVolcano (version 1.14)
819 (87).

820 **4.13.3 Cell cycle analysis**

821 Spearman correlation between normalized scaled read counts for each sample for all genes (as
822 one vector) and each time point of the reference microarray time course published by Bozdech
823 *et al*. (48) (3D7 smoothed, retrieved from PlasmoDB) were tested. Spearman's coefficients rho
824 for each time point of this RNA-Seq time course and each time point of the reference data set
825 where plotted using ggcorrplot (version 0.1.3) (88). For each time point of this RNA-Seq
826 dataset, the rho coefficients where then plotted against the time points of the reference data set
827 and the FKBP35^{WT} and FKBP35^{KO} data were fitted separately to the linearized sinusoidal $A *$
828 $sin\left(\frac{2\pi}{53}time\right) + B * cos\left(\frac{2\pi}{53}time\right) + C$ using R lm function. The time point matching best to
829 the FKBP35$^{\mathbf{WT}}$ and FKBP35$^{\mathbf{KO}}$ samples for each time point of the RNA-Seq time course was

taken as the maximum of this fitted function. Both fitted functions were F-tested (using R function var.test using both fitted model as applied to the FKBP35^{KO} data) to test whether the FKBP35^{WT} and FKBP35^{KO} data correlated with the reference data set (48) in a significantly different way, which would indicate a cell cycle shift if statistically significant. Only the last time point showed such a significant difference.

Acknowledgements

We thank Vera Mitesser and Ron Dzikowski for guidance on the SUnSET experiments and David Fidock for providing the parasite line Dd2-B2 used for the attempted resistance selection. We are grateful to the Polyomics facility at the University of Glasgow for processing the samples for RNA-Seq. This work was supported by the Swiss National Foundation (grant number 310030_200683), the Wolfson Merit Royal Society Award, the Wellcome Trust Investigator Award 110166 and Wellcome Trust Center Award 104111, and by the Singapore Ministry of Education (grant number MOE-T2EP30120-0015).

Author contributions

B.T.T. designed and performed experiments, analyzed and interpreted the data, and wrote the original draft of the manuscript. J.M.D. and S.T. performed and interpreted CETSA experiments. Z.B. supervised these experiments and provided resources. F.A. analyzed RNA-Seq data. M.M. supervised these experiments and provided resources for RNA-Seq data generation. A.P. performed immunofluorescence assays. K.B. performed and analyzed proteomics experiments supervised by A.S. C.Gu. and M.R. performed and interpreted hypoxanthine incorporation assays. C.Gr. edited the manuscript. N.M.B.B. conceived the study, designed and supervised experiments, provided resources, and wrote the manuscript. All authors contributed to the final editing of the manuscript.

Declaration of interests

The authors declare no competing interests.

859 **Figures and legends**

860

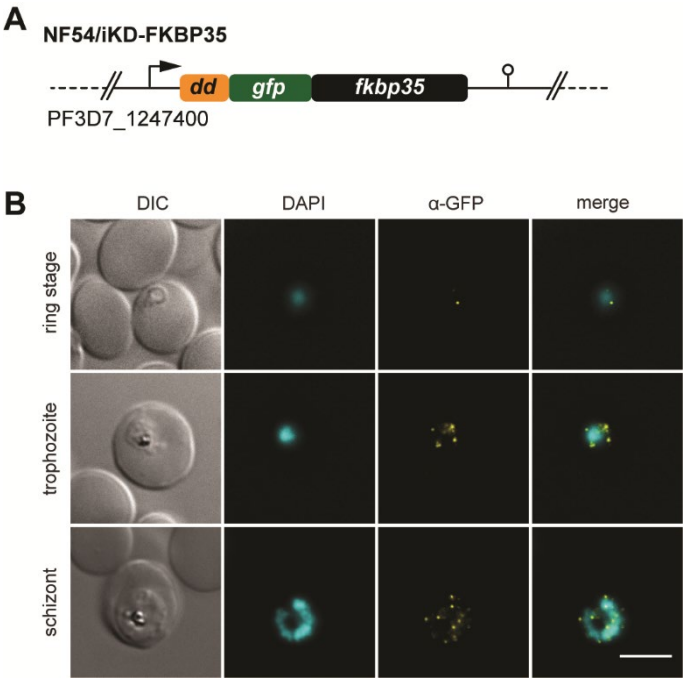

861

862 **Figure 1: Localization of *Pf*FKBP35 in NF54/iKD-FKBP35 parasites.**

863 **(A)** Schematic of the N-terminally modified *fkbp35* locus in NF54/iKD-FKBP35 parasites. *dd*,
864 destabilization domain. *gfp*, *green fluorescent protein*. **(B)** Localization of *Pf*FKBP35 in
865 NF54/iKD-FKBP35 parasites at the ring, trophozoite and schizont stage assessed by
866 immunofluorescence. DNA was stained with DAPI. Representative images are shown. Scale
867 bar: 5 µm. DIC, differential interference contrast.

868

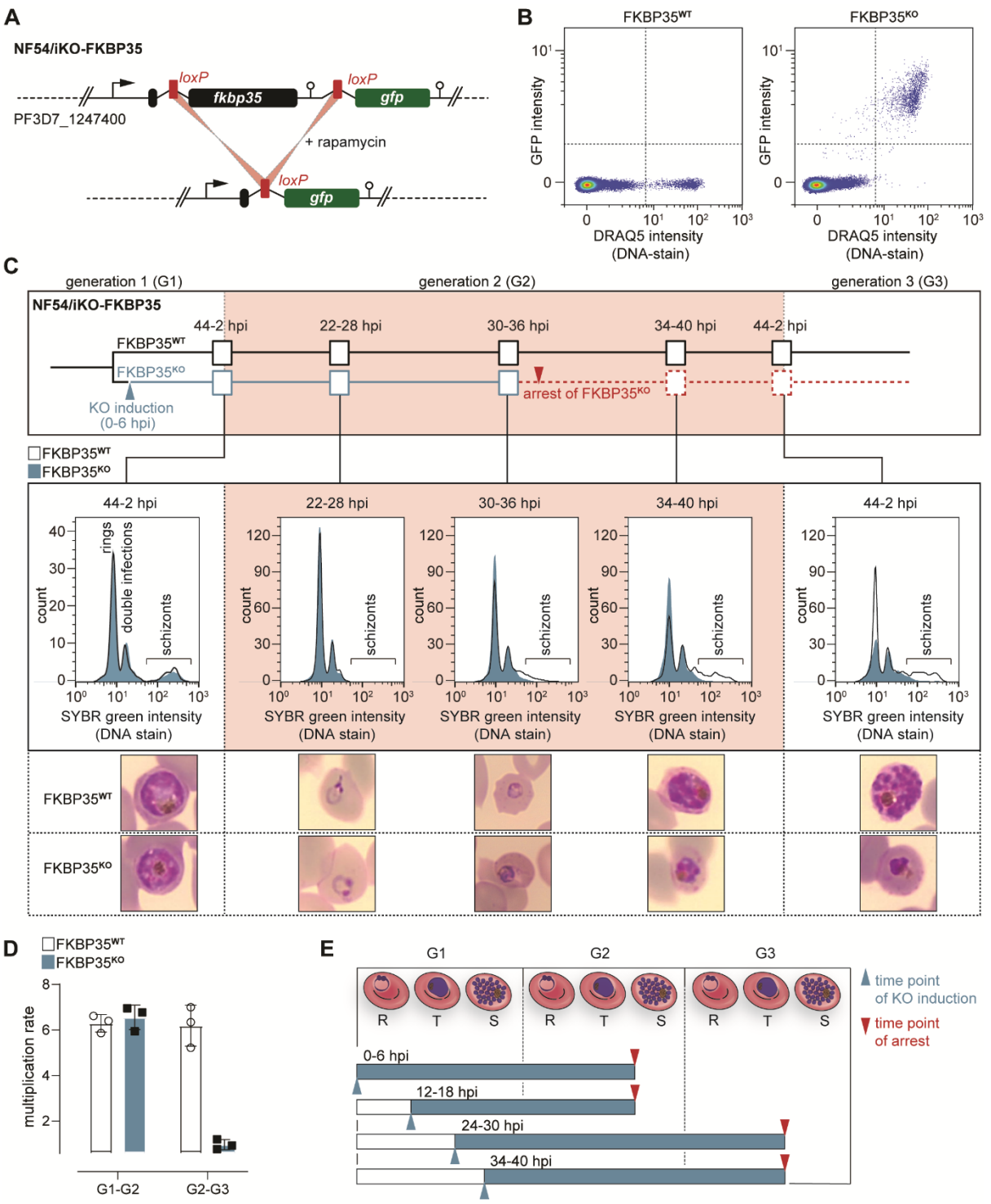

Figure 2. *Pf*FKBP35 depletion causes delayed parasite death.

(A) Schematic of the modified *fkbp35* locus in NF54/iKO-FKBP35 parasites before and after *loxP* recombination. *gfp*, *green fluorescent protein*. **(B)** Flow cytometry plot showing GFP expression in G1 schizonts of FKBP35^{KO} and FKBP35^{WT}. DNA was stained with DRAQ5. **(C)** Time course showing the development of NF54/iKO-FKBP35 parasites. Upper panel:

875 Schematic of the experimental setup. Middle panel: DNA content of the populations assessed
876 by flow cytometry based on the SYBR Green intensity. Lower panel: Giemsa-stained blood
877 smears. The knockout was induced at 0-6 hpi. Representative data of three biological replicates
878 are shown. **(D)** Multiplication rates of FKBP35^{KO} and FKBP35^{WT} parasites from generation 1
879 to generation 2 (G1-G2) and G2-G3. The knockout was induced at 0-6 hpi. Multiplication rates
880 were determined using flow cytometry. Data points represent the multiplication rates from G1-
881 G2 and G2-G3. n=3, error bars represent the standard error of the mean. **(E)** Schematic showing
882 time point of growth arrest (red arrow) following *Pf*FKBP35 knock-out at different hpi (blue
883 arrow). R, ring stage; T, trophozoite stage; S, schizont stage.
884

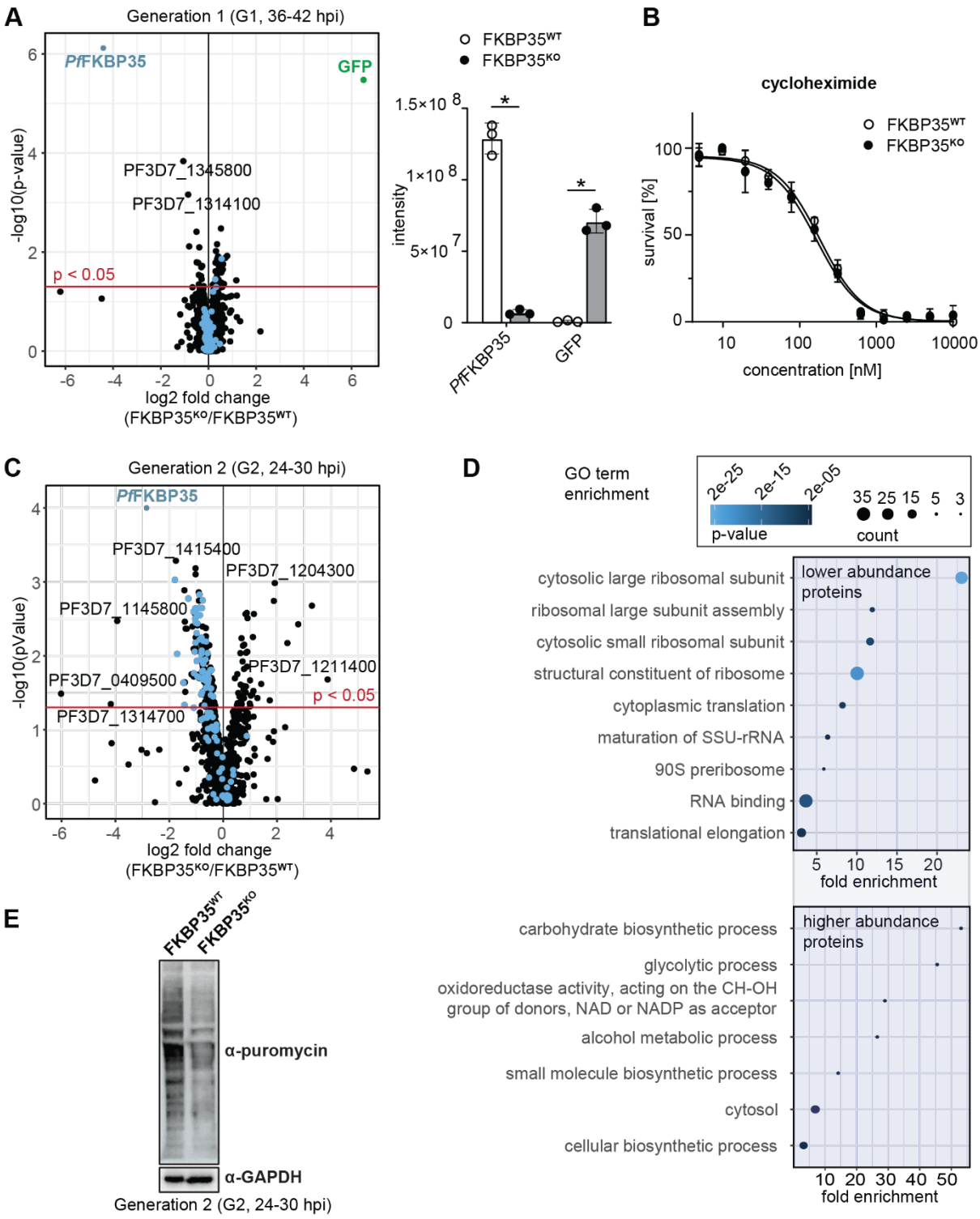

Figure 3. *Pf*FKBP35 is crucial for ribosome homeostasis and protein translation.

(A) Left panel: Proteome analysis of schizonts (36-42 hpi) in G1. The volcano plot shows change in protein abundance in FKBP35^{KO} compared to FKBP35^{WT}. Ribosomal proteins are highlighted in blue, n=3. Right panel: Relative difference in *Pf*FKBP35 and GFP abundance expressed as signal intensity measured by mass spectrometry. n=3, error bars represent the

892 standard error of the mean. **(B)** Dose-response effect of the translation inhibitor cycloheximide
893 on FKBP35^{KO} and FKBP35^{WT} parasites. The knockout was induced at 0-6 hpi and parasites
894 were subsequentially exposed to cycloheximide for 48 h. Parasite survival was quantified by
895 flow cytometry. n=3, error bars represent the standard error of the mean. **(C)** Proteome analysis
896 of trophozoites (24-30 hpi) in G2. The volcano plot shows change in protein abundance in
897 FKBP35^{KO} compared to FKBP35^{WT}. Ribosomal proteins are highlighted in blue. n=3. **(D)** GO
898 enrichment analysis of significantly deregulated proteins in FKBP35^{KO} trophozoites in G2. GO
899 enrichment analysis was performed using the PANTHER "Overrepresentation Test" with the
900 test type "Fisher's Exact" and the correction method "False Discovery Rate". **(E)** Assessment
901 of translation activity using SUnSET. FKBP35^{KO} and FKBP35^{WT} trophozoites of G2 were
902 incubated with puromycin for 1 hour. Incorporated puromycin was detected using an α-
903 puromycin antibody. α-GAPDH served as loading control. n=3, a representative Western blot
904 is shown.
905

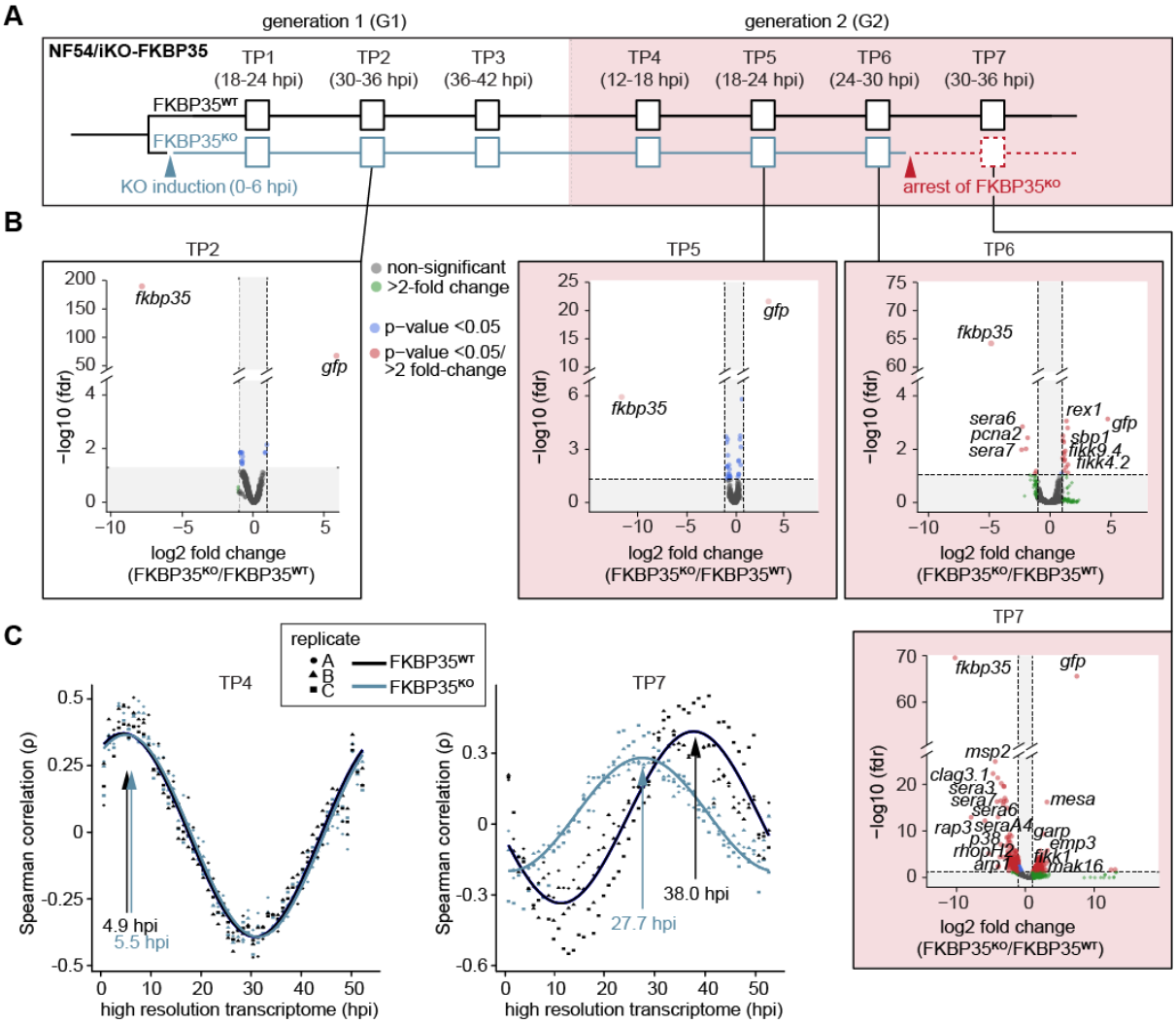

Figure 4. The knockout of *Pf*FKBP35 remains silent at the transcriptomic level.

(A) Setup of the RNA-Seq experiment. RNA was collected at seven indicated time points (TP). **(B)** Volcano plots show differential gene expression between FKBP35^{KO} and FKBP35^{WT} parasites. Genes are color-coded according to the fold change and fdr (false discovery rate), n=3. **(C)** Mapping of FKBP35^{KO} and FKBP35^{WT} transcriptomes to a high-resolution reference (48). Spearman rank coefficients (ρ) show correlation between the sampled transcriptomes and the reference data set (48). The time points with the highest correlation coefficient are indicated.

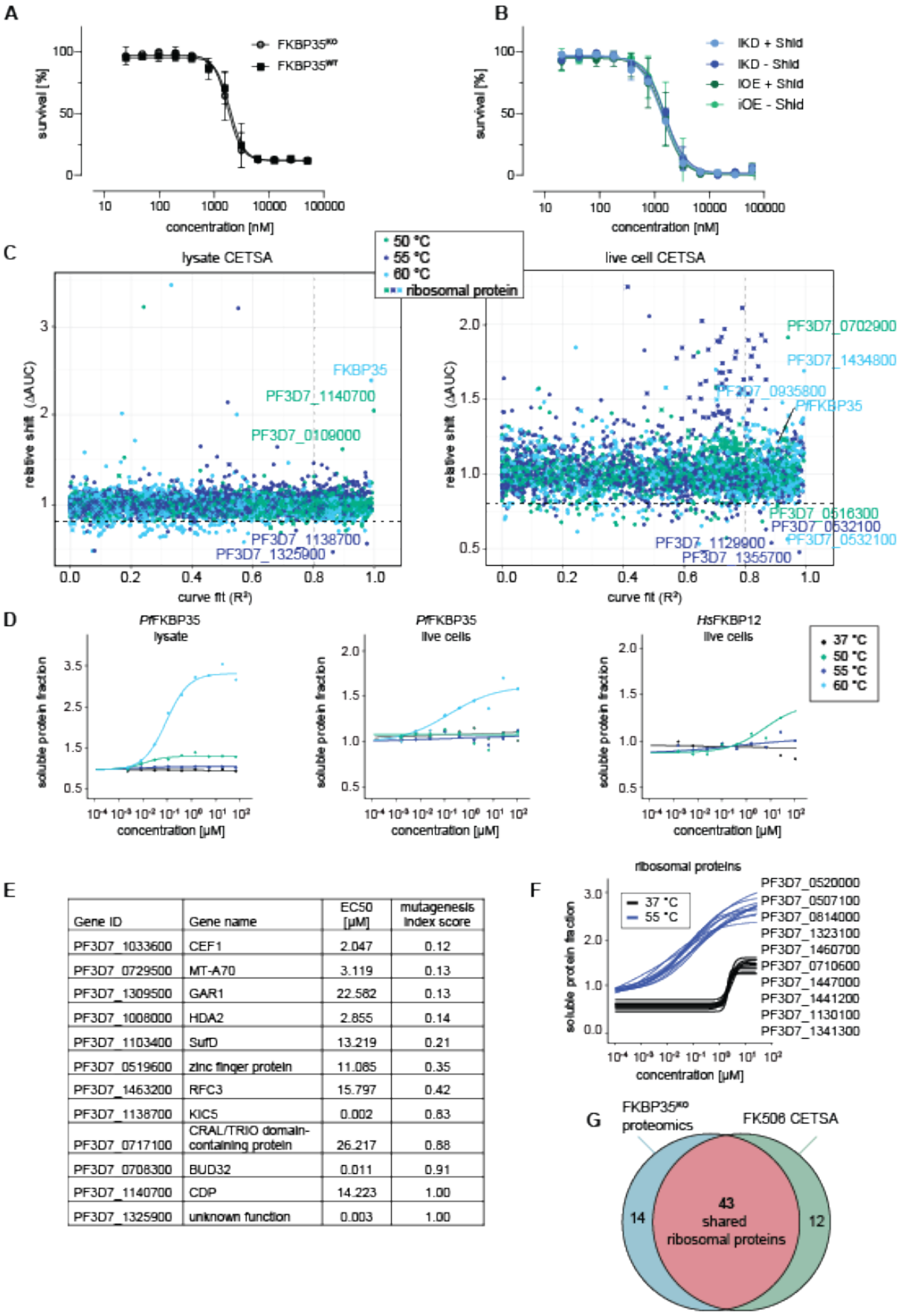

Gene ID	Gene name	EC50 [µM]	mutagenesis index score
PF3D7_1033600	CEF1	2.047	0.12
PF3D7_0729500	MT-A70	3.119	0.13
PF3D7_1309500	GAR1	22.582	0.13
PF3D7_1008000	HDA2	2.855	0.14
PF3D7_1103400	SufD	13.219	0.21
PF3D7_0519600	zinc finger protein	11.085	0.35
PF3D7_1463200	RFC3	15.797	0.42
PF3D7_1138700	KIC5	0.002	0.83
PF3D7_0717100	CRAL/TRIO domain-containing protein	26.217	0.88
PF3D7_0708300	BUD32	0.011	0.91
PF3D7_1140700	CDP	14.223	1.00
PF3D7_1325900	unknown function	0.003	1.00

Figure 5. CETSA identifies FK506 interaction partners.

917 **(A)** Dose-response effect of FK506 on FKBP35^{KO} and FKBP35^{WT} parasites. The knockout was
918 induced at 0-6 hpi and parasites were exposed to FK506 for 48 h. n=3, error bars represent the
919 standard error of the mean. **(B)** Dose-response effect of FK506 on NF54/iKD-FKBP35 and
920 NF54/iOE-FKBP35 parasites in presence and absence of Shield-1 (Shld). Parasites were split
921 at 0-6 hpi and subsequentially treated with Shld or the vehicle control EtOH. Data points
922 represent the mean of three and two independent biological replicates for the NF54/iOE-
923 FKBP35 and NF54/iKD-FKBP35 cell line, respectively. Error bars represent the standard error
924 of the mean. **(C)** CETSA results. The relative shift in protein abundance (area under the curve
925 of heat-challenged samples normalized against the non-denaturing control, ΔAUC) as a
926 function of R^2 (goodness of fit as a measure for the dose-response effect). The dashed lines
927 indicate an arbitrary cutoff of 3 times the median absolute deviation (MAD) of each dataset and
928 $R^2 = 0.8$. Three different temperatures were used for protein denaturation (indicated by colors).
929 **(D)** Dose-dependent stabilization of *P. falciparum* and human FKBPs detected using lysate and
930 live cell CETSA. Bullets represent the abundance of non-denatured proteins in response to
931 increasing FK506 concentrations under thermal challenge relative to the DMSO control. Colors
932 indicate the temperatures used for heat challenge; the black curve represents the non-denaturing
933 (37 °C) control. **(E)** Proteins with the most pronounced stability shift under thermal challenge
934 in the lysate CETSA experiment are listed. The EC50 is the concentration at which the half-
935 maximal effect of the FK506-induced thermal stabilization is reached. The mutagenesis index
936 score determined by Zhang *et al*. (23) is a measure to predict if a protein is essential for asexual
937 growth: 0 = essential, 1 = non-essential. **(F)** Fitted live cell CETSA curves of 10 representative
938 ribosomal proteins at 37 °C and 55 °C. Ribosomal proteins show a FK506 dose-dependent
939 increase in soluble protein fraction. **(G)** Venn diagram showing the overlap between ribosomal
940 proteins deregulated in the *Pf*FKBP35 knock-out cell line (less abundant in G2 FKBP^{KO}
941 trophozoites determined by proteomics) and the ribosomal proteins stabilized by FK506 in live
942 cell CETSA. The number of factors identified in either or both assays is indicated.
943

944 **Supplementary figures and legends**

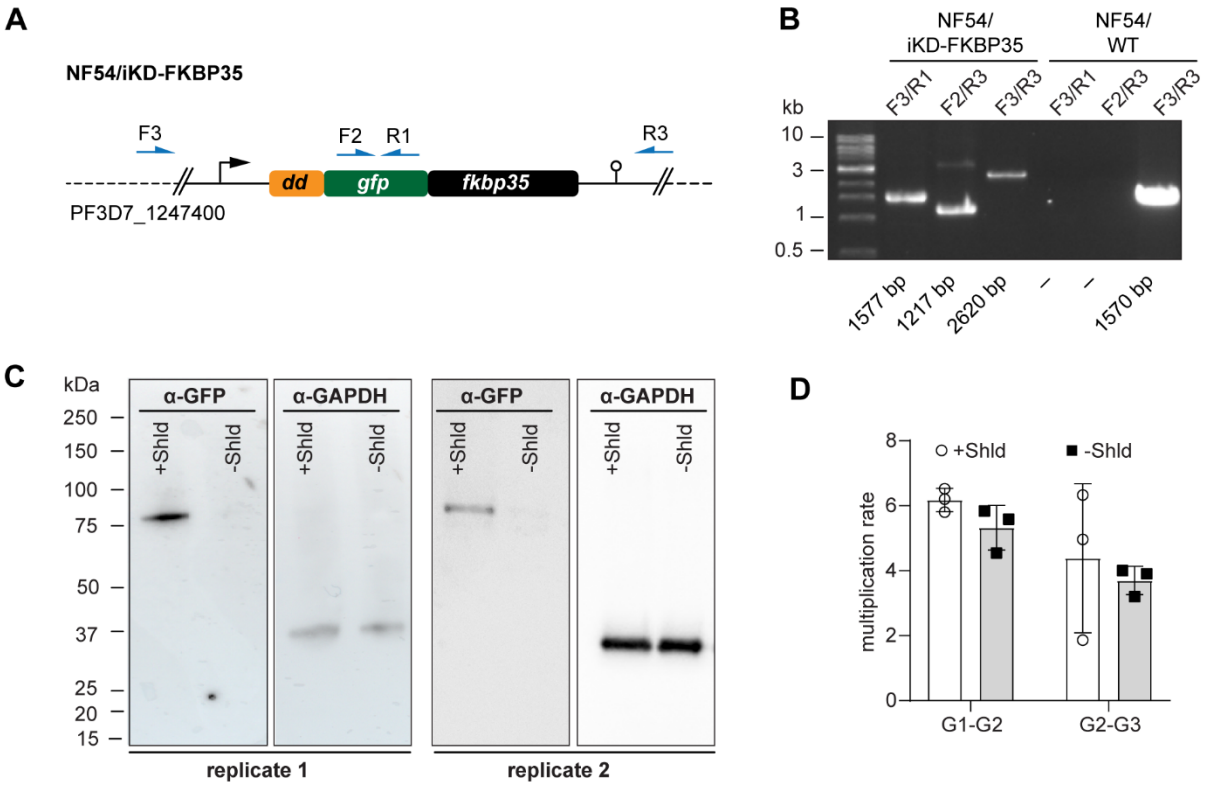

945

946

947 **Figure S1. Characterization of NF54/iKD-FKBP35 parasites.**

948 **(A)** Schematic of the modified *fkbp35* locus (PF3D7_1247400) in NF54/iKD-FKBP35
949 parasites. The 5'-end of *fkbp35* was tagged with the sequences of a destabilization domain (*dd*)
950 and a green fluorescent protein (*gfp*). The DD tag allows regulating protein levels post-
951 translationally using the stabilizing compound Shield-1 (Shld) (36, 37). Names and binding
952 sites of the primers used for diagnostic PCRs are indicated. **(B)** Diagnostic PCRs performed on
953 gDNA of NF54/FKBP35 iKD parasites to confirm correct editing of the locus. PCRs performed
954 on NF54/WT gDNA served as control. Numbers at the bottom indicate expected fragement
955 sizes. **(C)** Expression levels of the DD-GFP-FKBP35 fusion protein were assessed by Western
956 blot. Parasite cultures were split at 0-6 hpi and treated with Shld or the vehicle control EtOH.
957 Protein lysates were collected 40 hours later. α-GAPDH served as loading control. The expected
958 size of the DD-GFP-FKBP35 fusion protein is 74.2 kDa. **(D)** Multiplication rates of NF54/iKD-
959 FKBP35 parasites from generation 1 to generation 2 (G1-G2) and G2-G3. Parasites were split
960 at 0-6 hpi and treated with Shld or the vehicle control EtOH. Multiplication rates were
961 determined using flow cytometry. Data points represent the multiplication rates from G1-G2
962 and G2-G3, respectively. n=3; error bars represent the standard error of the mean.

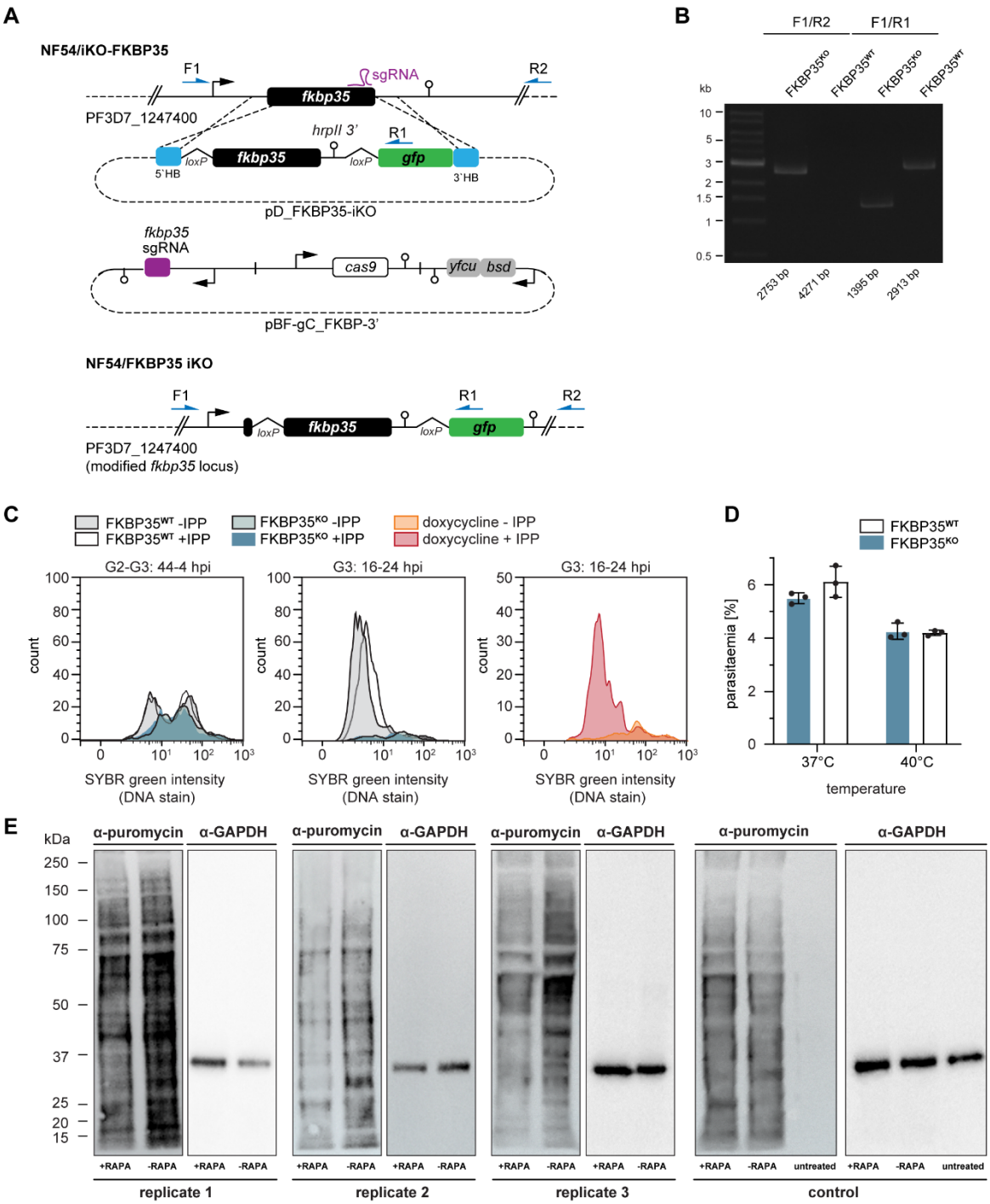

963

964 **Figure S2. CRISPR/Cas9-based generation of transgenic parasite lines.**

965 **(A)** Schematic of the wild type *fkbp35* locus (PF3D7_1247400) and the two plasmids used for
966 CRISPR/Cas9 gene editing (pD_FKBP35-iKO and pBF-gC_FKBP-3') to generate the
967 modified *fkbp35* locus of NF54/iKO-FKBP35 parasites. The modification consists of an intron
968 containing a *loxP* site that was introduced after the first 38 bp of the coding sequence and an
969 *hrpII* terminator inserted after the stop codon followed by another *loxP* site and a *gfp* sequence.
970 The sequence flanked by the *loxP* sites was recodonized to prevent homologous recombination

971 during gene editing. Names and binding sites of the primers used for diagnostic PCRs are
972 indicated. **(B)** Diagnostic PCRs on gDNA of NF54/iKO-FKBP35 parasites confirm correct
973 locus editing and rapamycin-induced *loxP* recombination. Numbers at the bottom indicate the
974 expected band sizes. **(C)** DNA content analysis of FKBP35$^{\mathbf{KO}}$ and FKBP35$^{\mathbf{WT}}$ parasites in
975 presence or absence of isopentenyl pyrophosphate (IPP)-supplementation. Disruption of
976 isoprenoid precursor biosynthesis in the apicoplast – the only essential function of this organelle
977 – is a known cause for delayed death in *P. falciparum* (41, 42). Inhibition of isoprenoid
978 synthesis by doxycycline can thus be restored by supplementing the parasite culture medium
979 with the isoprenoid precursor IPP (89). However, IPP supplementation did not alter the fate of
980 FKBP35$^{\mathbf{KO}}$ cells, demonstrating that their death in G2 is independent of apicoplast-dependent
981 processes as shown by DNA content analysis. Doxycycline-treated wild-type parasites rescued
982 by IPP-supplementation served as positive control**.** The knockout was induced at 0-6 hpi.
983 Representative data of three biological replicates are shown. **(D)** Parasite survival after
984 exposure to 40 °C for 6 h. Given the reported interactions of *Pf*FKBP35 with heat shock protein
985 70 (HSP70) and HSP90 (19, 21), we tested the parasite`s response to heat stress. *Pf*HSP70 is
986 required to ensure parasite survival under heat shock conditions by stabilizing the digestive
987 vacuole membrane trough binding to phosphatidylinositol 3-phosphate (90). Despite this
988 association, we did not detect altered heat-susceptibility between FKBP35$^{\mathbf{KO}}$ and FKBP35$^{\mathbf{WT}}$
989 cells. The knockout was induced at 0-6 hpi. n=3, error bars represent the standard error of the
990 mean**.** **(E)** Assessment of translation rates using SUnSET. FKBP35^{KO} and FKBP35^{WT}
991 trophozoites of G1 were incubated with puromycin for 1 hour. Incorporated puromycin was
992 detected using an α-puromycin antibody; α-GAPDH served as loading control. Replicate 3 is
993 also shown in main figure 3 (mirrored). The control was performed using an NF54/DiCre
994 parasite line. Untreated control parasites were cultured in absence of puromycin, confirming
995 the specificity of the α-puromycin antibody.

996

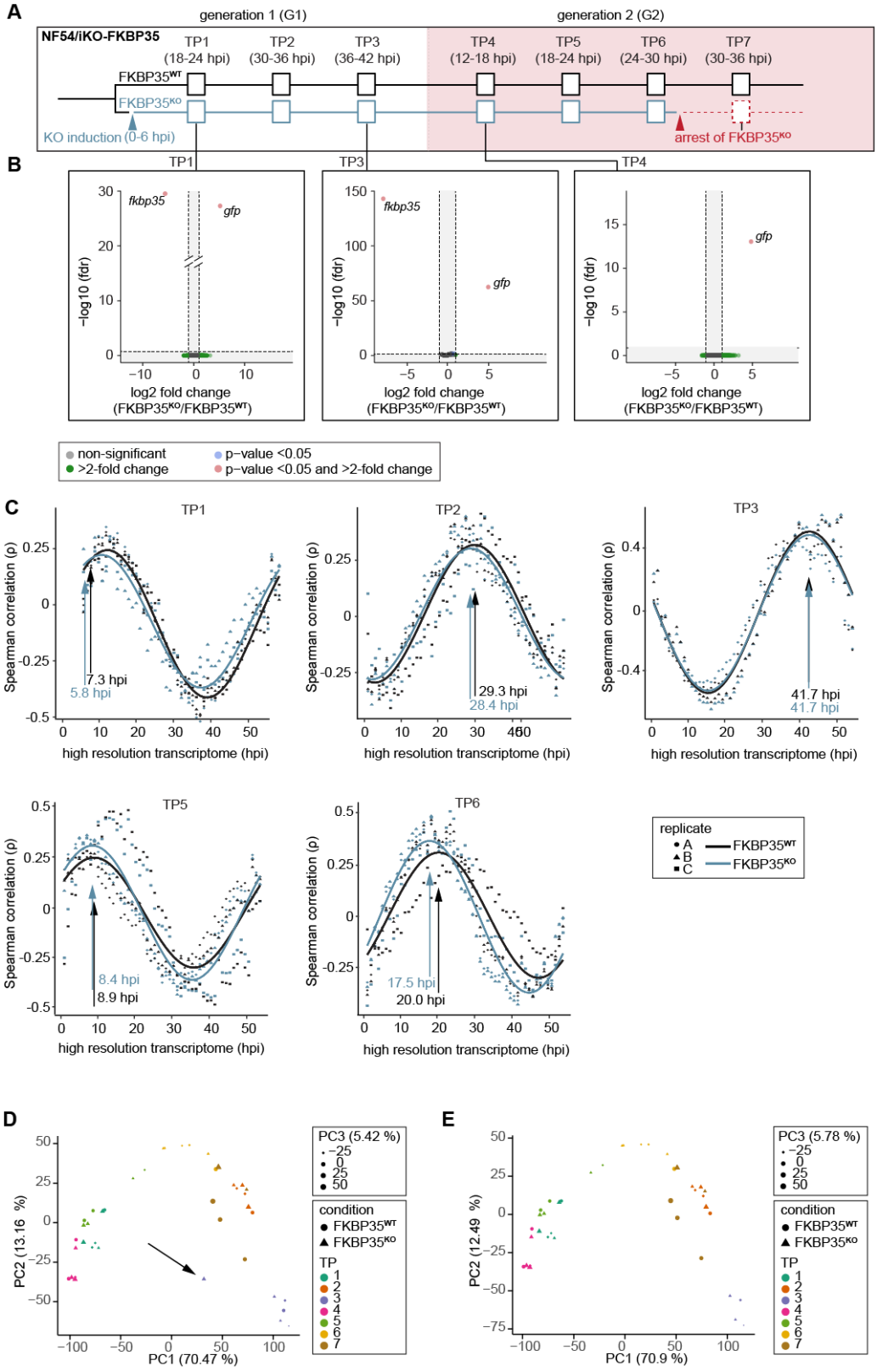

997

998 **Figure S3. Transcriptomics reveals a cell cycle arrest of FKBP35^{KO} parasites.**

999 **(A)** Schematic of the experimental setup. The knockout was induced at 0-6 hpi. RNA was
1000 collected at indicated time points (TPs). **(B)** Volcano plots show differential gene expression
1001 between FKBP35^{KO} and FKBP35^{WT} parasites. Genes are color-coded according to the fold

1002 change and fdr (false discovery rate), n=3. **(C)** Mapping of FKBP35^{KO} and FKBP35^{WT}
1003 transcriptomes to a high-resolution reference data set (48). Spearman rank coefficients (ρ)
1004 describe the correlation between the sampled transcriptomes and the reference data set. The
1005 time points with the highest correlation coefficient are indicated. **(D)** Principal component
1006 analysis (PCA) of RNA-Seq data by condition and time point (TP). The outlier at TP3
1007 (highlighted by an arrow) was removed from the analysis. **(E)** PCA of RNA-Seq data by
1008 condition and time point without the TP3 outlier mentioned in (D). Exclusion of this sample
1009 did not affect the overall pattern.

1010

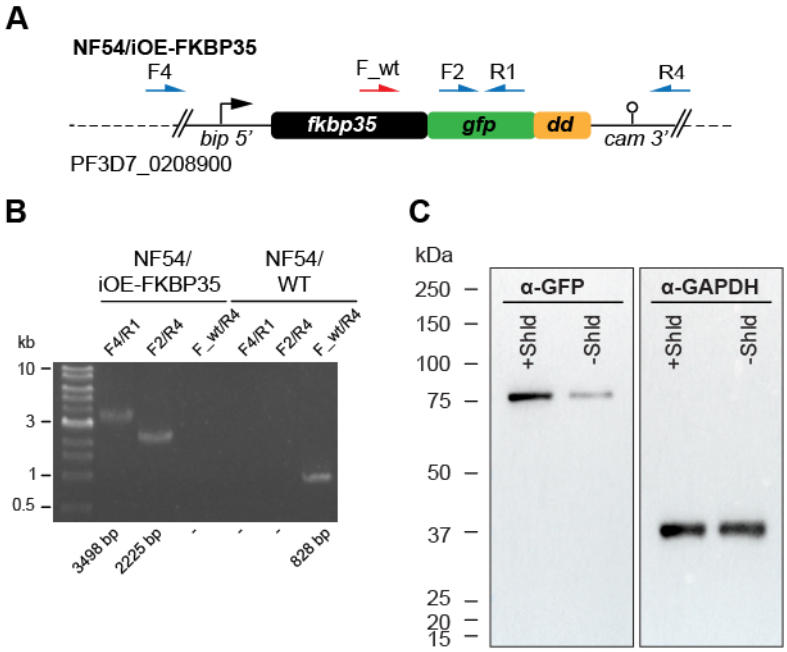

Figure S4. Characterization of NF54/iOE-FKBP35 parasites.

(A) Schematic of the modified *p230p* locus (PF3D7_0208900) in NF54/iOE-FKBP35 parasites, in which the overexpression cassette was introduced. This cassette consists of a *bip* promoter upstream of coding sequences of *fkbp35*, green fluorescent protein (*gfp*) and destabilization domain (*dd*), followed by the *cam 3'* region. Names and binding sites of the primers used for diagnostic PCRs are indicated. The primer F_wt only binds the unmodified *p230p* sequence. **(B)** Diagnostic PCRs performed on gDNA of NF54/iOE-FKBP35 parasites to confirm correct editing of the locus. PCRs performed on NF54/WT gDNA served as control. Numbers at the bottom indicate the expected band sizes. **(C)** Expression levels of the FKBP35-GFP-DD fusion protein were assessed by Western blot. Parasite cultures were split at 0-6 hpi and treated with Shield or the vehicle control EtOH. Protein lysates were collected 40 h later. α-GAPDH served as loading control. The expected size of the FKBP35-GFP-DD fusion protein is 74.2 kDa.

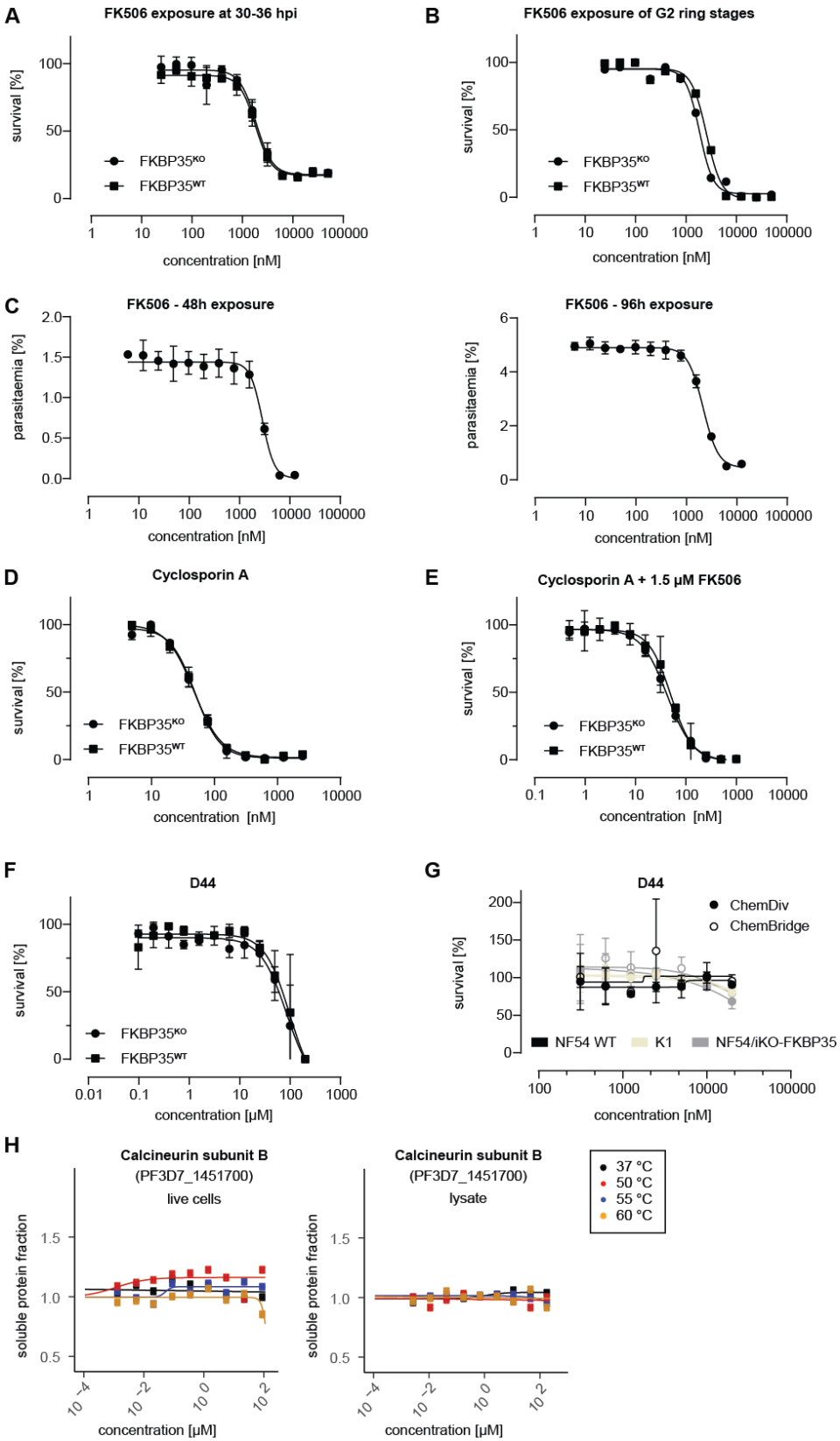

Figure S5. FKBP-targeting drugs fail at inhibiting parasite *Pf*FKBP35.

(A) Dose-response effect of FK506 on FKBP35^{KO} and FKBP35^{WT} parasites. The knockout was induced at 0-6 hpi and parasites were exposed to FK506 at 30-36 hpi. Survival rates were

1029 measured by flow cytometry in G2. n=3, error bars represent the standard error of the mean.
1030 **(B)** Dose-response effect of FK506 on FKBP35^{KO} and FKBP35^{WT} parasites. The knockout was
1031 induced at 34-40 hpi in G1. Ring stage parasites of G2 were exposed to FK506 for 48 hours
1032 and survival rates were measured by flow cytometry in G3. Data points represent survival rates
1033 measured in a single experiment performed in technical duplicates. **(C)** Dose-response effect of
1034 FK506 on FKBP35^{WT} parasites over two IDCs. Parasites at 0-6 hpi were exposed to FK506 and
1035 incubated for 96 hours. Parasitaemia was measured by flow cytometry after 48 hours and 96
1036 hours. Medium containing the appropriate drug concentrations was changed after 48 hours. n=3,
1037 error bars represent the standard error of the mean. **(D)** Dose-response effect of cyclosporin A
1038 on FKBP35^{KO} and FKBP35^{WT} parasites. The knockout was induced at 0-6 hpi. Parasites were
1039 exposed to cyclosporin A for 48 hours. n=3, error bars represent the standard error of the mean.
1040 **(E)** Dose-response effect of cyclosporin A in combination with a constant FK506 concentration
1041 on FKBP35^{KO} and FKBP35^{WT} parasites. The knockout was induced at 0-6 hpi. Parasites were
1042 subsequently exposed to cyclosporin A and 1.5 µM FK506 for 48 h. n=3, error bars represent
1043 the standard error of the mean. **(F)** Dose-response effect of D44 on FKBP35^{KO} and FKBP35^{WT}.
1044 The knockout was induced at 0-6 hpi and parasites were exposed to D44 for 48 hours thereafter.
1045 Survival rates were determined using flow cytometry. n=3, error bars represent the standard
1046 error of the mean. **(G)** Dose-response effect of D44 on NF54 WT, K1 and NF54/iKO-FKBP35
1047 parasites after 72 h exposure. Survival rates were determined using a hypoxanthine
1048 incorporation assay. Data points represent the mean of two technical replicates. Error bars
1049 represent the standard error of the mean. **(H)** Effect of FK506 on calcineurin subunit B
1050 determined by lysate and live cell CETSA. Bullets represent the abundance of non-denatured
1051 proteins in response to increasing FK506 concentrations under thermal challenge relative to a
1052 DMSO control. Colors indicate the temperatures used for protein denaturation; the black curve
1053 represents the non-denaturing control.

1054

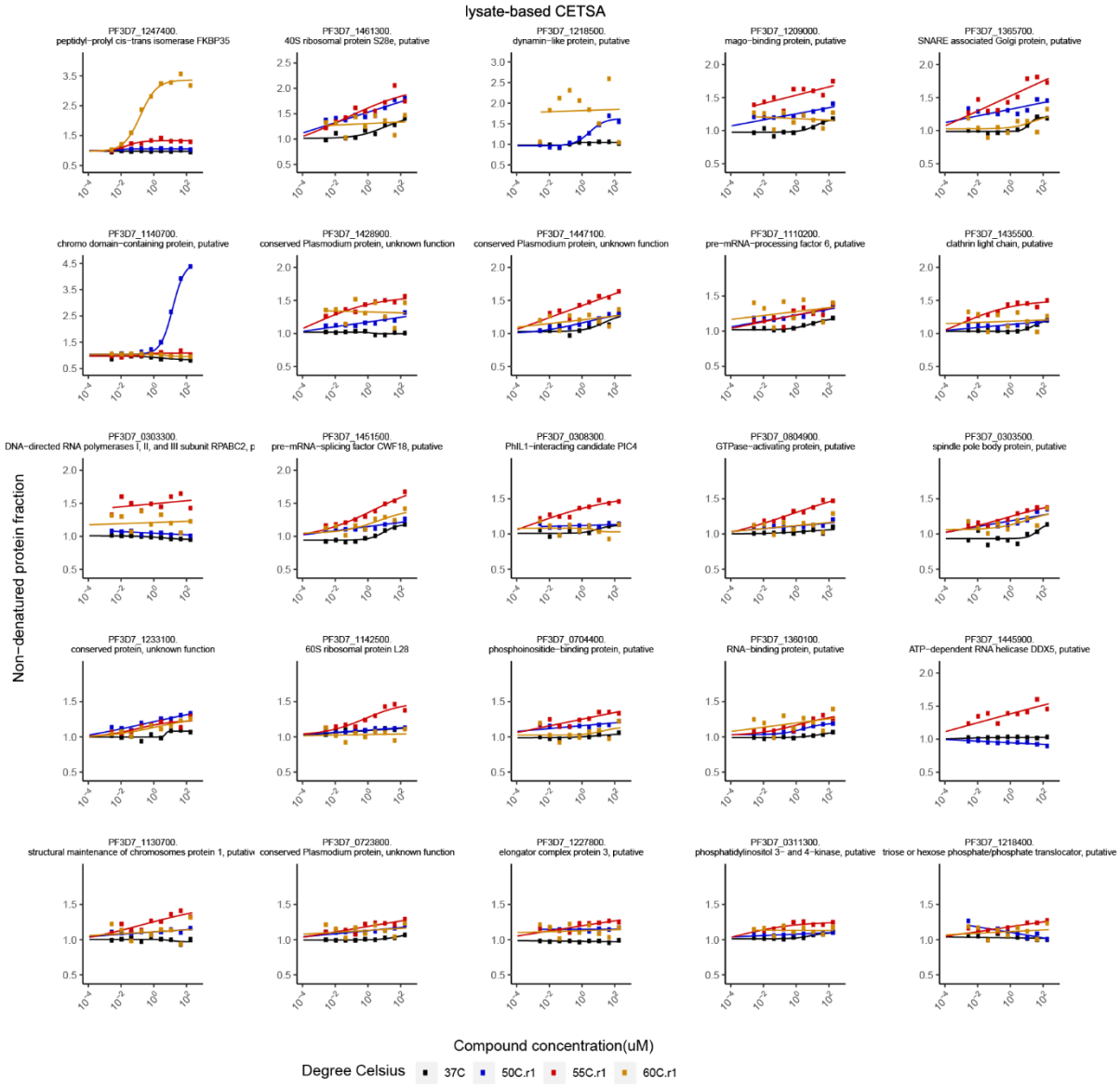

Figure S6. Putative FK506 interaction partners identified by protein lysate-based CETSA.

Proteins with an area under the curve (ΔAUC in protein lysate-based CETSA) greater than two median absolute deviations and an R^2 greater than 0.8 are listed. Bullets represent the abundance of non-denatured proteins in response to increasing FK506 concentrations under thermal challenge relative to a DMSO control. Colors indicate the temperatures used for protein denaturation; the black curve represents the non-denaturing control.

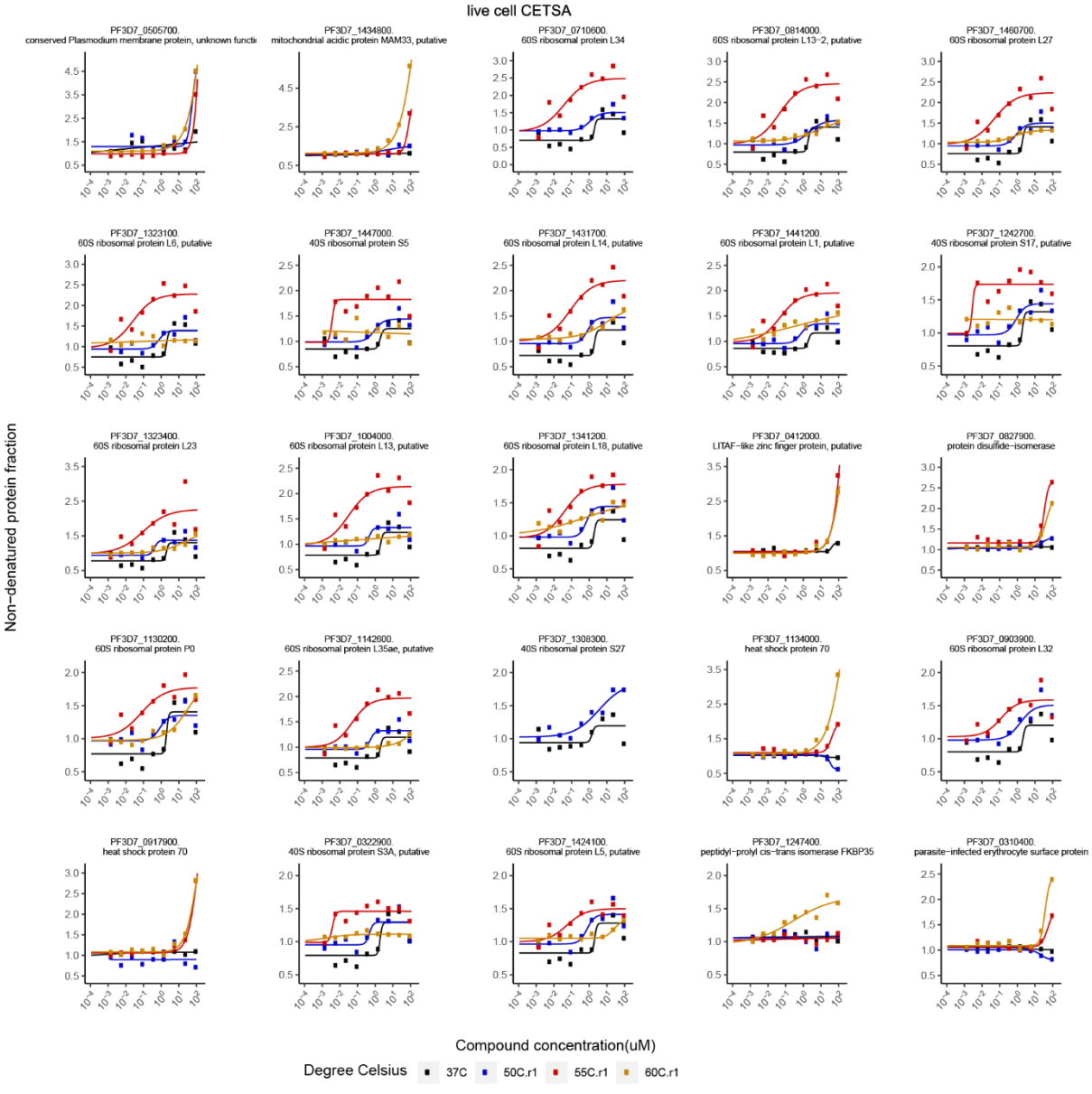

Figure S7. Putative FK506 interaction partners identified by live cell CETSA.

Proteins with an area under the curve (ΔAUC in live cell CETSA) greater than two median absolute deviations and an R^2 greater than 0.8 are listed. Bullets represent the abundance of non-denatured proteins in response to increasing FK506 concentrations under thermal challenge relative to a DMSO control. Colors indicate the temperatures used for heat challenge; the black curve represents the non-denaturing control.

1072 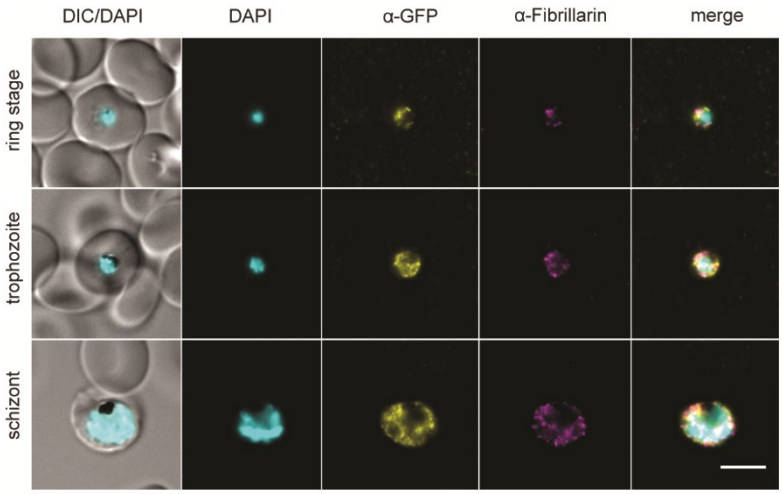

1073 **Figure S8. *Pf*FKBP35 localizes near fibrillarin-dense nuclear regions.**

1074 Localization of *Pf*FKBP35 (GFP) and fibrillarin in NF54/iKD-FKBP35 parasites at the ring,
1075 trophozoite and schizont stage assessed by immunofluorescence. DNA was stained with DAPI.
1076 Representative images are shown. Scale bar: 5 µm. DIC, differential interference contrast.

1077

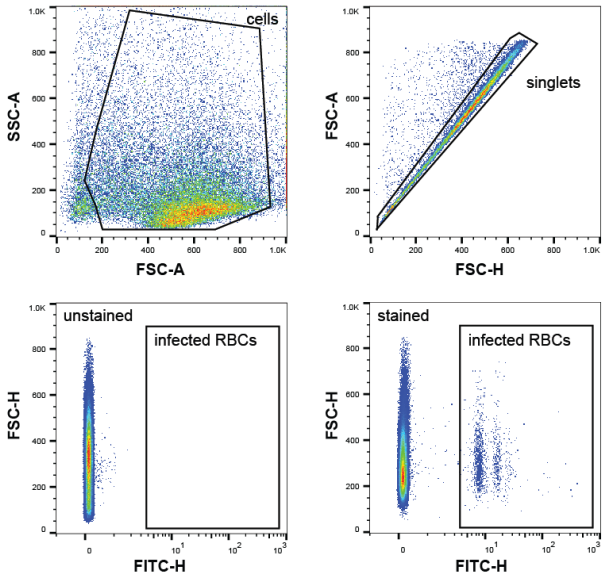

Figure S9. Gating strategy of flow cytometry data.

Representative flow cytometry plots of formaldehyde/glutaraldehyde-fixed parasite cultures are shown. The first plot shows the gate to distinguish cells from small debris (SSC-A vs. FSC-A). The 'singlets' gate (FSC-A vs. FSC-H) removes events with more than one cells. SYBR Green fluorescence intensity is used to identify parasite-infected RBCs (FSC-H vs. FITC-H). SSC, side scatter. FSC, forward scatter. FITC, fluorescein-5-isothiocyanate. A, area. H, height.

1086 **Table S1.** Mass spectrometry data comparing the proteomes of FKBP35^{KO} and FKBP35^{WT}
1087 parasites.

1088 **Table S2.** RNA-seq data comparing the transcriptomes of FKBP35^{KO} and FKBP35^{WT}
1089 parasites.

1090 **Table S3.** CETSA data showing the relative abundance of soluble proteins under non-
1091 denaturing and denaturing conditions in response to increasing FK506 concentrations.

1092 **Table S4.** Oligonucleotides used in this study.

1093

1094 **References**

1095 1. WHO. World malaria report 2021. Geneva: WHO; 2021.

1096 2. Ippolito MM, Moser KA, Kabuya JB, Cunningham C, Juliano JJ. Antimalarial Drug
1097 Resistance and Implications for the WHO Global Technical Strategy. Curr Epidemiol Rep.
1098 2021;8(2):46-62.

1099 3. Bell A, Wernli B, Franklin RM. Roles of peptidyl-prolyl cis-trans isomerase and
1100 calcineurin in the mechanisms of antimalarial action of cyclosporin A, FK506, and rapamycin.
1101 Biochem Pharmacol. 1994;48(3):495-503.

1102 4. Bharatham N, Chang MW, Yoon HS. Targeting FK506 binding proteins to fight
1103 malarial and bacterial infections: current advances and future perspectives. Curr Med Chem.
1104 2011;18(12):1874-89.

1105 5. Monaghan P, Bell A. A Plasmodium falciparum FK506-binding protein (FKBP) with
1106 peptidyl-prolyl cis-trans isomerase and chaperone activities. Mol Biochem Parasitol.
1107 2005;139(2):185-95.

1108 6. Bell A, Monaghan P, Page AP. Peptidyl-prolyl cis-trans isomerases (immunophilins)
1109 and their roles in parasite biochemistry, host-parasite interaction and antiparasitic drug
1110 action. Int J Parasitol. 2006;36(3):261-76.

1111 7. Kolos JM, Voll AM, Bauder M, Hausch F. FKBP Ligands-Where We Are and Where to
1112 Go? Front Pharmacol. 2018;9:1425.

1113 8. Kang CB, Hong Y, Dhe-Paganon S, Yoon HS. FKBP family proteins: immunophilins
1114 with versatile biological functions. Neurosignals. 2008;16(4):318-25.

1115 9. Bose S, Weikl T, Bügl H, Buchner J. Chaperone function of Hsp90-associated
1116 proteins. Science. 1996;274(5293):1715-7.

1117 10. Furutani M, Ideno A, Iida T, Maruyama T. FK506 binding protein from a thermophilic
1118 archaeon, methanococcus thermolithotrophicus, has chaperone-like activity in vitro.
1119 Biochemistry. 2000;39(10):2822.

1120 11. Wehrens XH, Lehnart SE, Huang F, Vest JA, Reiken SR, Mohler PJ, et al. FKBP12.6
1121 deficiency and defective calcium release channel (ryanodine receptor) function linked to
1122 exercise-induced sudden cardiac death. Cell. 2003;113(7):829-40.

1123 12. Cameron AM, Steiner JP, Roskams AJ, Ali SM, Ronnett GV, Snyder SH. Calcineurin
1124 associated with the inositol 1,4,5-trisphosphate receptor-FKBP12 complex modulates Ca2+
1125 flux. Cell. 1995;83(3):463-72.

1126 13. Wang T, Li BY, Danielson PD, Shah PC, Rockwell S, Lechleider RJ, et al. The
1127 immunophilin FKBP12 functions as a common inhibitor of the TGF beta family type I
1128 receptors. Cell. 1996;86(3):435-44.

1129 14. Ahearn IM, Tsai FD, Court H, Zhou M, Jennings BC, Ahmed M, et al. FKBP12 binds
1130 to acylated H-ras and promotes depalmitoylation. Mol Cell. 2011;41(2):173-85.

1131 15. Yang WM, Yao YL, Seto E. The FK506-binding protein 25 functionally associates with
1132 histone deacetylases and with transcription factor YY1. Embo j. 2001;20(17):4814-25.

1133 16. Kasahara K, Nakayama R, Shiwa Y, Kanesaki Y, Ishige T, Yoshikawa H, et al. Fpr1,
1134 a primary target of rapamycin, functions as a transcription factor for ribosomal protein
1135 genes cooperatively with Hmo1 in Saccharomyces cerevisiae. PLoS Genet.
1136 2020;16(6):e1008865.

1137 17. Dolinski K, Muir S, Cardenas M, Heitman J. All cyclophilins and FK506 binding
1138 proteins are, individually and collectively, dispensable for viability in Saccharomyces
1139 cerevisiae. Proc Natl Acad Sci U S A. 1997;94(24):13093-8.

1140 18. Cardenas ME, Zhu D, Heitman J. Molecular mechanisms of immunosuppression by
1141 cyclosporine, FK506, and rapamycin. Curr Opin Nephrol Hypertens. 1995;4(6):472-7.

1142 19. Leneghan D, Bell A. Immunophilin-protein interactions in Plasmodium falciparum.
1143 Parasitology. 2015;142(11):1404-14.

1144 20. Yoon HR, Kang CB, Chia J, Tang K, Yoon HS. Expression, purification, and
1145 molecular characterization of Plasmodium falciparum FK506-binding protein 35 (PfFKBP35).
1146 Protein expression and purification. 2007;53(1):179-85.

1147 21. Kumar R, Adams B, Musiyenko A, Shulyayeva O, Barik S. The FK506-binding protein
1148 of the malaria parasite, Plasmodium falciparum, is a FK506-sensitive chaperone with FK506-
1149 independent calcineurin-inhibitory activity. Mol Biochem Parasitol. 2005;141(2):163-73.

1150 22. Alag R, Bharatham N, Dong A, Hills T, Harikishore A, Widjaja AA, et al.
1151 Crystallographic structure of the tetratricopeptide repeat domain of Plasmodium falciparum
1152 FKBP35 and its molecular interaction with Hsp90 C-terminal pentapeptide. Protein Sci.
1153 2009;18(10):2115-24.

1154 23. Zhang M, Wang C, Otto TD, Oberstaller J, Liao X, Adapa SR, et al. Uncovering the
1155 essential genes of the human malaria parasite Plasmodium falciparum by saturation
1156 mutagenesis. Science. 2018;360(6388).

1157 24. Alag R, Qureshi IA, Bharatham N, Shin J, Lescar J, Yoon HS. NMR and
1158 crystallographic structures of the FK506 binding domain of human malarial parasite
1159 Plasmodium vivax FKBP35. Protein science : a publication of the Protein Society.
1160 2010;19(8):1577-86.

1161 25. Goh CKW, Silvester J, Wan Mahadi WNS, Chin LP, Ying LT, Leow TC, et al.
1162 Expression and characterization of functional domains of FK506-binding protein 35 from
1163 Plasmodium knowlesi. Protein Eng Des Sel. 2018;31(12):489-98.

1164 26. Bianchin A, Allemand F, Bell A, Chubb AJ, Guichou JF. Two crystal structures of the
1165 FK506-binding domain of Plasmodium falciparum FKBP35 in complex with rapamycin at high
1166 resolution. Acta crystallographica Section D, Biological crystallography. 2015;71(Pt 6):1319-
1167 27.

1168 27. Kotaka M, Ye H, Alag R, Hu G, Bozdech Z, Preiser PR, et al. Crystal structure of the
1169 FK506 binding domain of Plasmodium falciparum FKBP35 in complex with FK506.
1170 Biochemistry. 2008;47(22):5951-61.

1171 28. MacDonald CA, Boyd RJ. Computational insights into the suicide inhibition of
1172 Plasmodium falciparum Fk506-binding protein 35. Bioorg Med Chem Lett. 2015;25(16):3221-
1173 5.

1174 29. Harikishore A, Niang M, Rajan S, Preiser PR, Yoon HS. Small molecule Plasmodium
1175 FKBP35 inhibitor as a potential antimalaria agent. Sci Rep. 2013;3:2501.

1176 30. Harikishore A, Leow ML, Niang M, Rajan S, Pasunooti KK, Preiser PR, et al.
1177 Adamantyl derivative as a potent inhibitor of Plasmodium FK506 binding protein 35. ACS
1178 Med Chem Lett. 2013;4(11):1097-101.

1179 31. Rajan S, Yoon HS. Structural insights into Plasmodium PPIases. Front Cell Infect
1180 Microbiol. 2022;12:931635.

1181 32. MacDonald CA, Boyd RJ. Molecular docking study of macrocycles as Fk506-binding
1182 protein inhibitors. J Mol Graph Model. 2015;59:117-22.

1183 33. Deepa P, Thirumeignanam D. Understanding the potency of malarial ligand (D44) in
1184 plasmodium FKBP35 and modelled halogen atom (Br, Cl, F) functional groups. Journal of
1185 molecular graphics & modelling. 2020;97:107553.

1186 34. Atack TC, Raymond DD, Blomquist CA, Pasaje CF, McCarren PR, Moroco J, et al.
1187 Targeted Covalent Inhibition of Plasmodium FK506 Binding Protein 35. ACS Med Chem Lett.
1188 2020;11(11):2131-8.

1189 35. Monaghan P, Leneghan DB, Shaw W, Bell A. The antimalarial action of FK506 and
1190 rapamycin: evidence for a direct effect on FK506-binding protein PfFKBP35. Parasitology.
1191 2017;144(7):869-76.

1192 36. Armstrong CM, Goldberg DE. An FKBP destabilization domain modulates protein
1193 levels in Plasmodium falciparum. Nature methods. 2007;4(12):1007-9.

1194 37. Banaszynski LA, Chen LC, Maynard-Smith LA, Ooi AG, Wandless TJ. A rapid,
1195 reversible, and tunable method to regulate protein function in living cells using synthetic
1196 small molecules. Cell. 2006;126(5):995-1004.

1197 38. Collins CR, Das S, Wong EH, Andenmatten N, Stallmach R, Hackett F, et al. Robust
1198 inducible Cre recombinase activity in the human malaria parasite Plasmodium falciparum
1199 enables efficient gene deletion within a single asexual erythrocytic growth cycle. Mol
1200 Microbiol. 2013;88(4):687-701.

1201 39. Jones ML, Das S, Belda H, Collins CR, Blackman MJ, Treeck M. A versatile strategy
1202 for rapid conditional genome engineering using loxP sites in a small synthetic intron in
1203 Plasmodium falciparum. Sci Rep. 2016;6:21800.

1204 40. Kucharski M, Tripathi J, Nayak S, Zhu L, Wirjanata G, van der Pluijm RW, et al. A
1205 comprehensive RNA handling and transcriptomics guide for high-throughput processing of
1206 Plasmodium blood-stage samples. Malar J. 2020;19(1):363.

1207 41. Wiley JD, Merino EF, Krai PM, McLean KJ, Tripathi AK, Vega-Rodríguez J, et al.
1208 Isoprenoid precursor biosynthesis is the essential metabolic role of the apicoplast during
1209 gametocytogenesis in Plasmodium falciparum. Eukaryot Cell. 2015;14(2):128-39.

1210 42. Kennedy K, Cobbold SA, Hanssen E, Birnbaum J, Spillman NJ, McHugh E, et al.
1211 Delayed death in the malaria parasite Plasmodium falciparum is caused by disruption of
1212 prenylation-dependent intracellular trafficking. PLoS Biol. 2019;17(7):e3000376.

1213 43. Mi H, Ebert D, Muruganujan A, Mills C, Albou LP, Mushayamaha T, et al. PANTHER
1214 version 16: a revised family classification, tree-based classification tool, enhancer regions
1215 and extensive API. Nucleic Acids Res. 2021;49(D1):D394-d403.

1216 44. Boisvert FM, van Koningsbruggen S, Navascués J, Lamond AI. The multifunctional
1217 nucleolus. Nat Rev Mol Cell Biol. 2007;8(7):574-85.

1218 45. Plouffe D, Brinker A, McNamara C, Henson K, Kato N, Kuhen K, et al. In silico activity
1219 profiling reveals the mechanism of action of antimalarials discovered in a high-throughput
1220 screen. Proceedings of the National Academy of Sciences of the United States of America.
1221 2008;105(26):9059-64.

1222 46. Schmidt EK, Clavarino G, Ceppi M, Pierre P. SUnSET, a nonradioactive method to
1223 monitor protein synthesis. Nat Methods. 2009;6(4):275-7.

1224 47. Bonner JM, Boulianne GL. Diverse structures, functions and uses of FK506 binding
1225 proteins. Cellular signalling. 2017;38:97-105.

1226 48. Bozdech Z, Llinas M, Pulliam BL, Wong ED, Zhu J, DeRisi JL. The transcriptome of
1227 the intraerythrocytic developmental cycle of Plasmodium falciparum. PLoS biology.
1228 2003;1(1):E5.

1229 49. Barnum KJ, O'Connell MJ. Cell cycle regulation by checkpoints. Methods Mol Biol.
1230 2014;1170:29-40.

1231 50. Van Duyne GD, Standaert RF, Karplus PA, Schreiber SL, Clardy J. Atomic structure
1232 of FKBP-FK506, an immunophilin-immunosuppressant complex. Science.
1233 1991;252(5007):839-42.

1234 51. Paul AS, Saha S, Engelberg K, Jiang RH, Coleman BI, Kosber AL, et al. Parasite
1235 Calcineurin Regulates Host Cell Recognition and Attachment by Apicomplexans. Cell Host
1236 Microbe. 2015;18(1):49-60.

1237 52. Dumont FJ. FK506, an immunosuppressant targeting calcineurin function. Curr Med
1238 Chem. 2000;7(7):731-48.

1239 53. Desjardins RE, Canfield CJ, Haynes JD, Chulay JD. Quantitative assessment of
1240 antimalarial activity in vitro by a semiautomated microdilution technique. Antimicrob Agents
1241 Chemother. 1979;16(6):710-8.

1242 54. Dziekan JM, Yu H, Chen D, Dai L, Wirjanata G, Larsson A, et al. Identifying purine
1243 nucleoside phosphorylase as the target of quinine using cellular thermal shift assay. Sci
1244 Transl Med. 2019;11(473).

1245 55. Dziekan JM, Wirjanata G, Dai L, Go KD, Yu H, Lim YT, et al. Cellular thermal shift
1246 assay for the identification of drug-target interactions in the Plasmodium falciparum
1247 proteome. Nat Protoc. 2020;15(6):1881-921.

1248 56. Tan CSH, Go KD, Bisteau X, Dai L, Yong CH, Prabhu N, et al. Thermal proximity
1249 coaggregation for system-wide profiling of protein complex dynamics in cells. Science.
1250 2018;359(6380):1170-7.

1251 57. Ünal CM, Steinert M. FKBPs in bacterial infections. Biochim Biophys Acta.
1252 2015;1850(10):2096-102.

1253 58. Ng CL, Fidock DA. Plasmodium falciparum In Vitro Drug Resistance Selections and
1254 Gene Editing. Methods Mol Biol. 2019;2013:123-40.

1255 59. Kramer G, Patzelt H, Rauch T, Kurz TA, Vorderwülbecke S, Bukau B, et al. Trigger
1256 factor peptidyl-prolyl cis/trans isomerase activity is not essential for the folding of cytosolic
1257 proteins in Escherichia coli. J Biol Chem. 2004;279(14):14165-70.

1258 60. Gavigan CS, Kiely SP, Hirtzlin J, Bell A. Cyclosporin-binding proteins of Plasmodium
1259 falciparum. Int J Parasitol. 2003;33(9):987-96.

1260 61. Gudavicius G, Dilworth D, Serpa JJ, Sessler N, Petrotchenko EV, Borchers CH, et al.
1261 The prolyl isomerase, FKBP25, interacts with RNA-engaged nucleolin and the pre-60S
1262 ribosomal subunit. Rna. 2014;20(7):1014-22.

1263 62. Sydorskyy Y, Dilworth DJ, Halloran B, Yi EC, Makhnevych T, Wozniak RW, et al.
1264 Nop53p is a novel nucleolar 60S ribosomal subunit biogenesis protein. Biochem J.
1265 2005;388(Pt 3):819-26.

1266 63. Ferbitz L, Maier T, Patzelt H, Bukau B, Deuerling E, Ban N. Trigger factor in complex
1267 with the ribosome forms a molecular cradle for nascent proteins. Nature.
1268 2004;431(7008):590-6.

1269 64. Callebaut I, Mornon JP. Trigger factor, one of the Escherichia coli chaperone
1270 proteins, is an original member of the FKBP family. FEBS Lett. 1995;374(2):211-5.

1271 65. Dieckmann-Schuppert A, Hensel J, Schwarz RT. Studies on the effect of tunicamycin
1272 on erythrocytic stages of Plasmodium falciparum. Biochem Soc Trans. 1992;20(2):184s.

1273 66. Naik RS, Venkatesan M, Gowda DC. Plasmodium falciparum: the lethal effects of
1274 tunicamycin and mevastatin on the parasite are not mediated by the inhibition of N-linked
1275 oligosaccharide biosynthesis. Exp Parasitol. 2001;98(2):110-4.

1276 67. Awad D, Prattes M, Kofler L, Rössler I, Loibl M, Pertl M, et al. Inhibiting eukaryotic
1277 ribosome biogenesis. BMC Biol. 2019;17(1):46.

1278 68. Rodriguez-Corona U, Sobol M, Rodriguez-Zapata LC, Hozak P, Castano E. Fibrillarin
1279 from Archaea to human. Biol Cell. 2015;107(6):159-74.

1280 69. Thiry M, Lafontaine DL. Birth of a nucleolus: the evolution of nucleolar compartments.
1281 Trends in cell biology. 2005;15(4):194-9.

1282 70. Lambros C, Vanderberg JP. Synchronization of Plasmodium falciparum erythrocytic
1283 stages in culture. J Parasitol. 1979;65(3):418-20.

1284 71. Trager W, Jenson JB. Cultivation of malarial parasites. Nature. 1978;273(5664):621-
1285 2.

1286 72. Brancucci NMB, Gerdt JP, Wang C, De Niz M, Philip N, Adapa SR, et al.
1287 Lysophosphatidylcholine Regulates Sexual Stage Differentiation in the Human Malaria
1288 Parasite Plasmodium falciparum. Cell. 2017;171(7):1532-44.e15.

1289 73. Filarsky M, Fraschka SA, Niederwieser I, Brancucci NMB, Carrington E, Carrio E, et
1290 al. GDV1 induces sexual commitment of malaria parasites by antagonizing HP1-dependent
1291 gene silencing. Science. 2018;359(6381):1259-63.

1292 74. Knuepfer E, Napiorkowska M, van Ooij C, Holder AA. Generating conditional gene
1293 knockouts in Plasmodium - a toolkit to produce stable DiCre recombinase-expressing
1294 parasite lines using CRISPR/Cas9. Sci Rep. 2017;7(1):3881.

1295 75. Gibson DG, Young L, Chuang RY, Venter JC, Hutchison CA, 3rd, Smith HO.
1296 Enzymatic assembly of DNA molecules up to several hundred kilobases. Nat Methods.
1297 2009;6(5):343-5.

1298 76. Ashdown GW, Dimon M, Fan M, Sánchez-Román Terán F, Witmer K, Gaboriau DCA,
1299 et al. A machine learning approach to define antimalarial drug action from heterogeneous
1300 cell-based screens. Sci Adv. 2020;6(39).

1301 77. Tibúrcio M, Yang ASP, Yahata K, Suárez-Cortés P, Belda H, Baumgarten S, et al. A
1302 Novel Tool for the Generation of Conditional Knockouts To Study Gene Function across the
1303 Plasmodium falciparum Life Cycle. mBio. 2019;10(5).

1304 78. Thommen BT, Passecker A, Buser T, Hitz E, Voss TS, Brancucci NMB. Revisiting the
1305 Effect of Pharmaceuticals on Transmission Stage Formation in the Malaria Parasite
1306 Plasmodium falciparum. Frontiers in cellular and infection microbiology. 2022;12:802341.

1307 79. Thomas JA, Collins CR, Das S, Hackett F, Graindorge A, Bell D, et al. Development
1308 and Application of a Simple Plaque Assay for the Human Malaria Parasite Plasmodium
1309 falciparum. PLoS One. 2016;11(6):e0157873.

1310 80. Daubenberger CA, Tisdale EJ, Curcic M, Diaz D, Silvie O, Mazier D, et al. The N'-
1311 terminal domain of glyceraldehyde-3-phosphate dehydrogenase of the apicomplexan
1312 Plasmodium falciparum mediates GTPase Rab2-dependent recruitment to membranes. Biol
1313 Chem. 2003;384(8):1227-37.

1314 81. Ahrné E, Glatter T, Viganò C, Schubert C, Nigg EA, Schmidt A. Evaluation and
1315 Improvement of Quantification Accuracy in Isobaric Mass Tag-Based Protein Quantification
1316 Experiments. J Proteome Res. 2016;15(8):2537-47.

1317 82. Ritchie ME, Phipson B, Wu D, Hu Y, Law CW, Shi W, et al. limma powers differential
1318 expression analyses for RNA-sequencing and microarray studies. Nucleic Acids Res.
1319 2015;43(7):e47.

1320 83. McLean KJ, Jacobs-Lorena M. Plasmodium falciparum Maf1 Confers Survival upon
1321 Amino Acid Starvation. MBio. 2017;8(2).

1322 84. Kim D, Paggi JM, Park C, Bennett C, Salzberg SL. Graph-based genome alignment
1323 and genotyping with HISAT2 and HISAT-genotype. Nat Biotechnol. 2019;37(8):907-15.

1324 85. Aurrecoechea C, Brestelli J, Brunk BP, Dommer J, Fischer S, Gajria B, et al.
1325 PlasmoDB: a functional genomic database for malaria parasites. Nucleic Acids Res.
1326 2009;37(Database issue):D539-43.

1327 86. Love MI, Huber W, Anders S. Moderated estimation of fold change and dispersion for
1328 RNA-seq data with DESeq2. Genome Biol. 2014;15(12):550.

1329 87. Blighe K, Rana S, Lewis M. EnhancedVolcano: Publication-ready volcano plots with
1330 enhanced colouring and labeling. R package version 1.16.0.
1331 https://githubcom/kevinblighe/EnhancedVolcano. 2022.

1332 88. Kassambara A. ggcorrplot: Visualization of a Correlation Matrix using 'ggplot2'. R
1333 package version 0.1.3, . https://CRANR-projectorg/package=ggcorrplot. 2022.

1334 89. Yeh E, DeRisi JL. Chemical rescue of malaria parasites lacking an apicoplast defines
1335 organelle function in blood-stage Plasmodium falciparum. PLoS Biol. 2011;9(8):e1001138.

1336 90. Lu KY, Pasaje CFA, Srivastava T, Loiselle DR, Niles JC, Derbyshire E.
1337 Phosphatidylinositol 3-phosphate and Hsp70 protect Plasmodium falciparum from heat-
1338 induced cell death. Elife. 2020;9.

1339